Ore Geology Reviews 77 (2016) 57–71

Contents lists available at ScienceDirect

Ore Geology Reviews

journal homepage: www.elsevier.com/locate/oregeorev

# Origin of anomalously Ni-rich parental magmas and genesis of the Huangshannan Ni–Cu sulfide deposit, Central Asian Orogenic Belt, Northwestern China

Yun Zhao, Chunji Xue *, Xiaobo Zhao, Yongqiang Yang, Junjun Ke, Bo Zu, Guozhen Zhang

*State Key Laboratory of Geological Processes and Mineral Resources, China University of Geosciences, Beijing 100083, China*

ARTICLE INFO

*Article history:*
Received 18 August 2015
Received in revised form 3 February 2016
Accepted 8 February 2016
Available online 10 February 2016

*Keywords:*
Huangshannan Intrusion
Ni-rich parental magmas
Different magma pulses and types
Olivine compositional variation

ABSTRACT

The Huangshannan Ni–Cu sulfide deposit at the southern margin of the Central Asian Orogenic Belt (CAOB) is an important recent discovery in the Eastern Tianshan Region, Northwestern China. The Huangshannan Intrusion is composed of mafic and ultramafic rocks, and its websterite and lherzolite sequences host the sulfide orebodies. Olivine is the dominant mineral in the Huangshannan Intrusion, occurring as olivine inclusions hosted by pyroxene oikocrysts, as olivine crystals in magmatic sulfides, and as poikilitic crystals in the lherzolite. Small olivine inclusions always coexist with large poikilitic olivine crystals in the same sample, resulting in a heterogeneous texture on the scale of the oikocrysts. The Ni abundance ranges from 1540 to 3772 ppm in poikilitic olivine grains, from 2114 to 3740 ppm in olivine grains hosted by sulfide minerals, and from 2043 to 4023 ppm in olivine inclusions hosted by pyroxene oikocrysts. For the three types of olivine, the ranges in forsterite (Fo) content are 78.97–84.92 mol.%, 81.57–84.79 mol.%, and 80.33–84.68 mol.%, respectively. The Ni content of olivine in the lherzolite is anomalously high relative to the range found in most within plate olivine-bearing mafic-ultramafic rocks. The composition of olivine is controlled mainly by that of the parental magma, fractional crystallization and reactions with interstitial silicate and sulfide melts. Both fractional crystallization and reaction with interstitial silicate may cause a decrease in the Ni content of olivine. The possibility that Ni–Fe exchange causes the anomalously high Ni contents in olivine can be excluded because the olivine grains contained in sulfide have similar or lower Ni content than the olivine grains hosted in the silicate rock. Most of the olivine grains are unzoned, and they have anomalously high Ni contents throughout the crystal. Assuming a partition coefficient of Ni between olivine and silicate magma to be 7, the measured Ni content of olivine in the lherzolite (1540–4023 ppm with a mean of 2907 ppm) indicates that the parental magma contains 220–575 ppm (average of 415 ppm) Ni. This value is higher than that found in basaltic magmas that crystallized olivine with similar Fo contents compared to the Huangshannan Intrusion. As mentioned above, the symmetric and reproducible variations in both Fo and Ni contents from core to margin in most of the olivine grains cannot be explained by fractional crystallization and reactions with interstitial silicate or sulfide melts but may reflect the equilibration of the olivine with new fluxes of magma as the chamber was replenished. The anomalously Ni-rich composition of the parental magmas of the Huangshannan Intrusion, relative to those of many other mineralized olivine-bearing mafic-ultramafic intrusions, may be produced by upgrading and scavenging of metals from a previously formed sulfide melts by a moderately Ni-rich magma. The mass-balance calculations of PGE data indicate that the parental magma that formed lherzolite contains 0.04 ppb Os, 0.02 ppb Ir and 0.4 ppb Pd, whereas the parental magma that formed websterite has 0.02 ppb Os, 0.009 ppb Ir and 0.75 ppb Pd. Rayleigh modeling using PGE tenors indicates that the massive sulfides may be produced by monosulfide solid solution (MSS)-sulfide liquid fractionation from the magma that formed the websterite. Rayleigh modeling of Fo and Ni contents of olivine shows that the parental magma that formed the lherzolite has experienced previous sulfide segregation and olivine crystallization.



## 1. Introduction

Magmatic Ni–Cu deposits are commonly hosted by komatiite lavas or variably differentiated intrusions with a basaltic to high-Mg basaltic composition (e.g., Li et al., 2004; Barnes and Lightfoot, 2005). Olivine is often the dominant mineral in the host intrusion and its composition

* Corresponding author.
*E-mail address:* chunji.xue@cugb.edu.cn (C. Xue).

http://dx.doi.org/10.1016/j.oregeorev.2016.02.003
0169-1368/

is often directly related to that of the parental magma (Li et al., 2004; Su et al., 2012). Nickel and Mg are compatible during olivine crystallization whereas Fe is less compatible (Barnes and Lightfoot, 2005; Li et al., 2007). Thus, the forsterite (Fo) and Ni contents of olivine provide important constraints in understanding the sulfide saturation and segregation history and the evolution of the magma (Naldrett et al., 1984).

Sudbury, Jinchuan and Noril'sk are the three largest Ni–Cu sulfide ore deposit camps in the world, and they are related to magmas of basaltic to intermediate compositions (Naldrett, 1998; Li et al., 2004). The Ni contents in olivine from Jinchuan and Noril'sk range from 1515 to 2485 ppm (Li et al., 2004) and from 456 to 2281 ppm (Li et al., 2007), respectively. The Sudbury Deposits are thought to have been generated by meteorite impact (Lightfoot et al., 2001), and although there are co-genetic ultramafic intrusions that contain fresh olivine (e.g., Lightfoot et al., 1997; Corfu and Lightfoot, 1996), these rocks are not yet understood in the context of metallogenesis. Huangshandong, Huangshanxi and Tulaergen are the three largest Ni–Cu sulfide deposits in the Eastern Tianshan in Northwestern China. The Ni contents in olivine of these deposits range from 502 to 2695 ppm (Deng et al., 2012), from 346 to 1318 ppm (Zhang et al., 2011), and from 314 to 1886 ppm (Sun, 2009), respectively. In the adjacent Beishan terrane, the Ni contents in olivine from Ni–Cu sulfide deposits show a large variation from 1070 to 3461 ppm for Heishan (Xie et al., 2013), from 789 to 2961 ppm for Pobei (Xia et al., 2013), from 786 to 1087 ppm for Xuanwoling (Su et al., 2010), from 236 to 2672 ppm for Hongshishan (Su et al., 2009), and from 314 to 3771 ppm for Poshi (Su et al., 2011). Many magmatic ore-bearing intrusions have been found in the Emeishan Large Igneous Province and their Ni contents in olivine vary from 976 to 2176 ppm for Ni–Cu deposits (e.g., Limahe and Qingshuihe), from 1024 to 2543 ppm for Ni–Cu-PGE deposits (e.g., Qingkuangshan and Huangcaoping), and from 776 to 1775 ppm for PGE deposits (e.g., Jinbaoshan and Yanghewu, see summary in Guan et al., 2010). Compared to these deposits, the Ni contents of olivine in lherzolite from the Huangshannan Intrusion are significantly higher, ranging from 1540 to 4023 ppm with a mean of 2907 ppm. Furthermore, the Ni tenor (in 100% sulfides) ranges from 7.83 to 22.06% (mean of 14.10%) in the Huangshannan Deposit, which is much higher than found in many other important Ni–Cu deposits in the world, such as Noril'sk (7.06%, Naldrett, 2004), Jinchuan (10.41%, Chen et al., 2013) and Huangshandong Deposits (2.31%, Gao et al., 2013). The mechanisms accounting for the high Ni content of the olivine and of the sulfides in the Huangshannan Deposit are not fully understood.

In this paper, we report the results of a detailed study of olivine compositional variations in lherzolite from the Huangshannan Intrusion to better understand the evolution of the parental magma. A combination of olivine compositions and PGE variations is used to assess the origin of the parental magma and to evaluate whether it was anomalously Ni-rich. We use PGE to constrain both the nature of the different magma types and the sulfide mineralization processes in the magmatic conduit system. A genetic model for the Huangshannan Deposit is proposed.

## 2. Geologic background

The Central Asian Orogenic Belt (CAOB) extends more than 5000 km from the Pacific Ocean to the European Craton (Fig. 1a). The CAOB is a complex collage of continental fragments, Paleozoic island arc assemblages, remnants of oceanic crust, and assemblages of volcanic rock (Sengör et al., 1993; Jahn et al., 2004; Xiao et al., 2009). The Chinese Tianshan orogenic belt is located in the southern part of the CAOB. From south to north, this orogenic belt can be further divided into the South, Middle and North Tianshan terranes, separated by the South and North Tianshan faults (Fig. 1b). The eastern parts of the Middle Tianshan and North Tianshan terranes are referred to collectively as the Eastern Tianshan (Fig. 1b, Sun et al., 2013). From south to north in the Eastern Tianshan, the Middle Tianshan terrane and North Tianshan terrane are separated by the Northern Tianshan or Shaquanzi faults (Fig. 1b and c). To the south, the Middle Tianshan terrane is separated from the Beishan terrane by the North Tarim and Xingxingxia faults (Fig. 1b and c).

The Huangshan area is located in the eastern part of the Eastern Tianshan (Fig. 1b and c), and includes the Middle and North Tianshan terranes that are separated by the Shaquanzi fault (Fig. 1c). The Middle Tianshan terrane consists mainly of Precambrian basement complexes overlain by Paleozoic sedimentary and volcanic strata whereas the North Tianshan terrane is composed of abundant Paleozoic volcanic and sedimentary rocks (Gao et al., 2013). Carboniferous granodiorite plutons are widespread in the Middle Tianshan terrane, whereas Permian A-type granitoids are developed in the North Tianshan terrane (Fig. 1c, Mao et al., 2014).

The magmatic Ni–Cu deposits in the Huangshan area are hosted mainly in small mafic-ultramafic intrusions that are distributed between the NE-trending Kangguer-Huangshan and Shaquanzi faults (Fig. 1c). These faults are part of the tectonic framework and created space for the transportation of dense sulfide-bearing magma through a conduit system that underwent repeated transtension and transpression, which effectively pumped the sulfide-bearing magma into the space created by faulting (Lightfoot and Evans-Lamswood, 2015). The Huangshannan Intrusion is located at the middle part of the Kangguer-Huangshan fault (Fig. 1c).

## 3. Geology of the Huangshannan Deposit

The Huangshannan Intrusion is lens-shaped with an area of about 4 $km^2$ (Fig. 2). It intrudes the Carboniferous Gandun Formation that consists of biotite quartz schist, two-mica quartz schist and garnet-bearing biotite quartz schist (Wang et al., 1987). The Huangshannan Intrusion is composed of an ultramafic unit in the eastern part and a mafic unit in both the eastern and western parts (Fig. 2a). The ultramafic unit is composed of harzburgite, lherzolite, olivine websterite, websterite and hornblende websterite (Fig. 2a). The mafic unit is composed dominantly of norite, gabbro, hornblende gabbro and diorite (Fig. 2a). These rocks show mingling textures at the contact between these two units (Wang et al., 1987). Websterite fragments are found in the mafic unit (Fig. 2b), consistent with the mafic unit cutting the ultramafic package (Zhao et al., 2015). Lenticular, vein and irregular ultramafic fragments are found in the ultramafic unit, which implies that the intrusion was formed by the emplacement of multiple pulses of magma. For example, Fig. 2b illustrates that lherzolite fragments are enclosed by websterite; this suggests that the lherzolite and websterite were formed from different magma pulses.

There are 18 identified orebodies in the ultramafic unit, but no orebodies have been found in the mafic unit. Lenticular and vein-type Ni–Cu sulfide orebodies occur mainly within websterite and lherzolite at the base or in the lower parts of the ultramafic unit (Fig. 2b), and most of the orebodies are hosted in lherzolite. The sulfide mineralization is generally disseminated (1–30 wt.% sulfide) whereas semi-massive and massive sulfides (>50 wt.% sulfide) are rare. The massive and semi-massive sulfide accumulations are generally small with tabular, lenticular or pipe-like shapes and they are usually hosted in the websterite.

The sulfide minerals are mainly composed of pyrrhotite, pentlandite and chalcopyrite (Fig. 3c, d, e and f). They occur as irregular isolated patches of variable sizes that are interstitial to the silicate minerals (Fig. 3c, d, e and f). Pentlandite occurs as flames or thin veinlets within pyrrhotite or as distinct crystals (Fig. 3c and d). Chalcopyrite is generally developed at the edge of pyrrhotite and/or pentlandite crystals or as inclusions in these minerals (Fig. 3d, e and f). In a few cases, the massive sulfides occur as chalcopyrite-rich and pyrrhotite-rich zones (Fig. 3g). Such zones may result from the fractionation of sulfide melts to form a Fe-rich monosulfide solid solution (MSS) and a Cu-rich sulfide liquid (Barnes and Lightfoot, 2005).

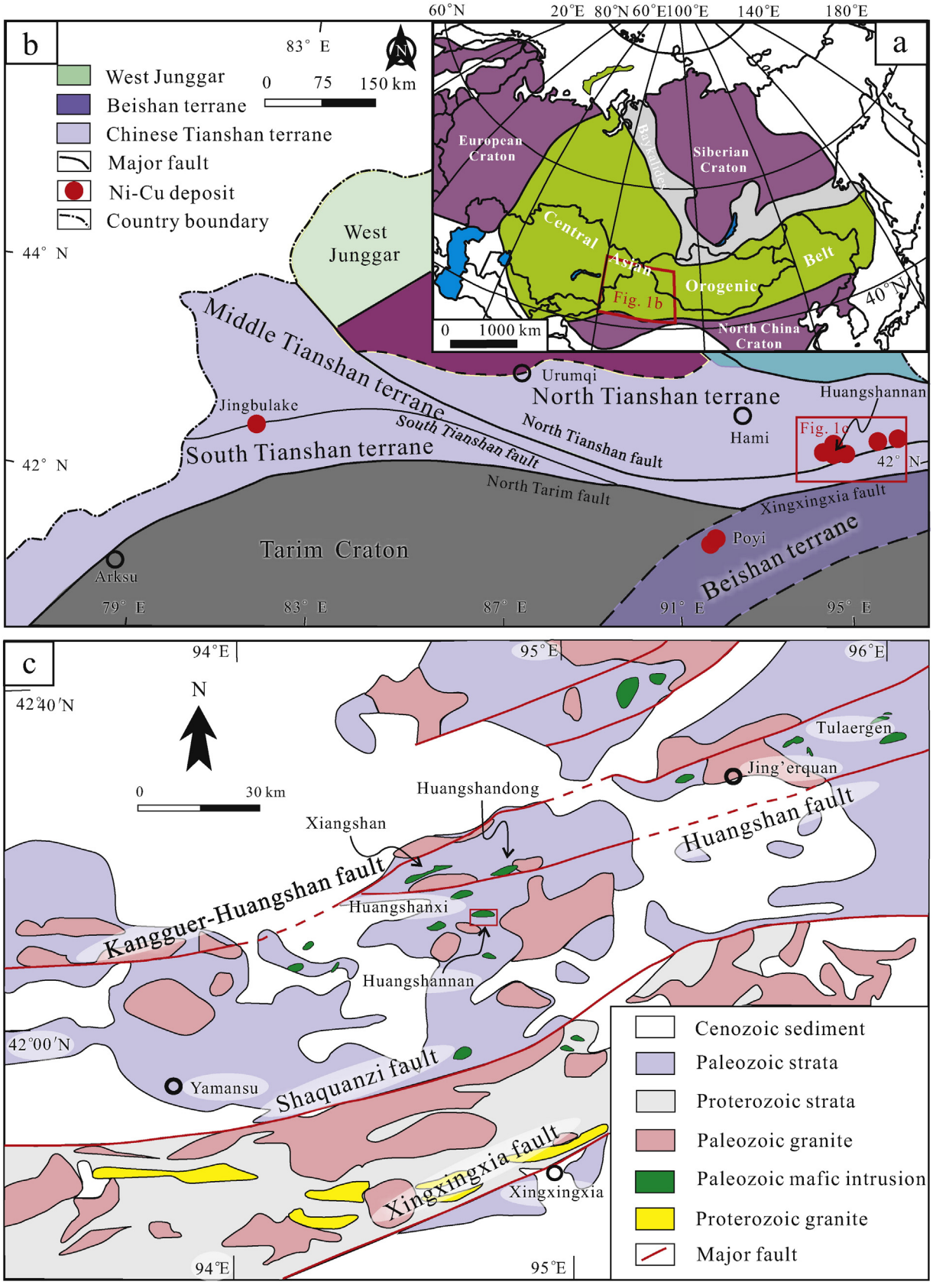


**Fig. 1.** (a) A simplified tectonic map of central Asia (modified from Jahn et al., 2004). (b) Geologic map of the Chinese Tianshan orogenic belt and distribution of magmatic Ni–Cu deposits (modified from Sun et al., 2013). (c) Simplified geologic map of the Huangshan area (modified from Wang et al., 2006 and Gao et al., 2013).

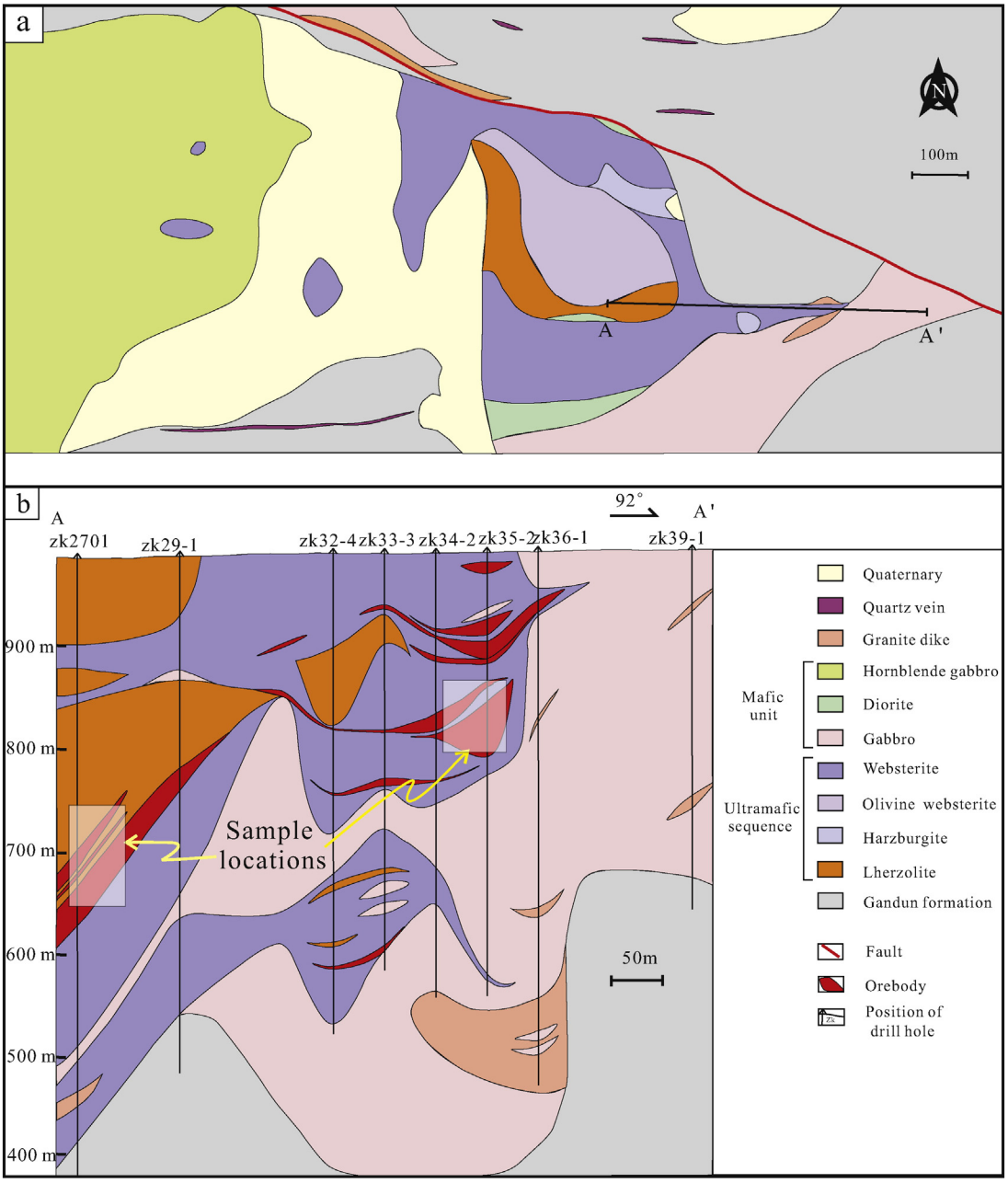


**Fig. 2.** (a) Simplified geologic map of the Huangshannan Intrusion. (b) A–A′ prospecting line of the Huangshannan Deposit (modified after Inner Mongolia Mineral Experimental Research Institute and Wang et al., 1987).

## 4. Types of olivine

Three types of olivine have been recognized in the Huangshannan Intrusion: (1) poikilitic crystals enclosing pyroxene (Fig. 4a, b, c, d and e), (2) olivine grains in sulfide (Fig. 4f and g), and (3) olivine inclusions in pyroxene oikocrysts (Fig. 4h). All three types of olivine have been observed in the ultramafic unit. Olivine inclusions and poikilitic olivine are most common in the ultramafic unit, whereas olivine grains enclosed in sulfides are rare. Poikilitic olivine crystals are large and rounded, varying from 2 to 5 mm in diameter (Fig. 4a, b, c, d and e). Olivine inclusions are much smaller, mostly <500 μm in diameter and irregular in shape (Fig. 4h). The olivine inclusions are randomly oriented in most samples from the Huangshannan Intrusion. Olivine grains in sulfide generally have subhedral to euhedral shapes and similar grain sizes to those that occur as olivine inclusions (Fig. 4f and g). Small olivine inclusions always coexist with large poikilitic olivine crystals in the same sample, resulting in a heterogeneous texture on the scale of the oikocrysts. The poikilitic olivines and olivine inclusions show intercumulate textures. Discrete grains of olivine are sometimes enclosed in sulfide.

Irregular-shaped olivine-rich clots termed “olivinite” are common in the picritic gabbro unit of the Talnakh Intrusion that hosts the Talnakh Ni–Cu sulfide deposits (Li et al., 2003). Olivinite possibly represents a xenolith of early olivine cumulate and thus the olivine in olivinite is always more primitive than the olivine in the gabbroic to picritic host rocks (Likhachev, 1994; Li et al., 2003). Olivinite is most common in the ultramafic unit, especially in the lherzolite (Fig. 3a and b), but it is rare in the mafic unit of the Huangshannan Intrusion.

## 5. Sampling and analytical methods

Samples for this study were collected from underground adits in the ultramafic unit of the Huangshannan Deposit (Fig. 2b). The lherzolite

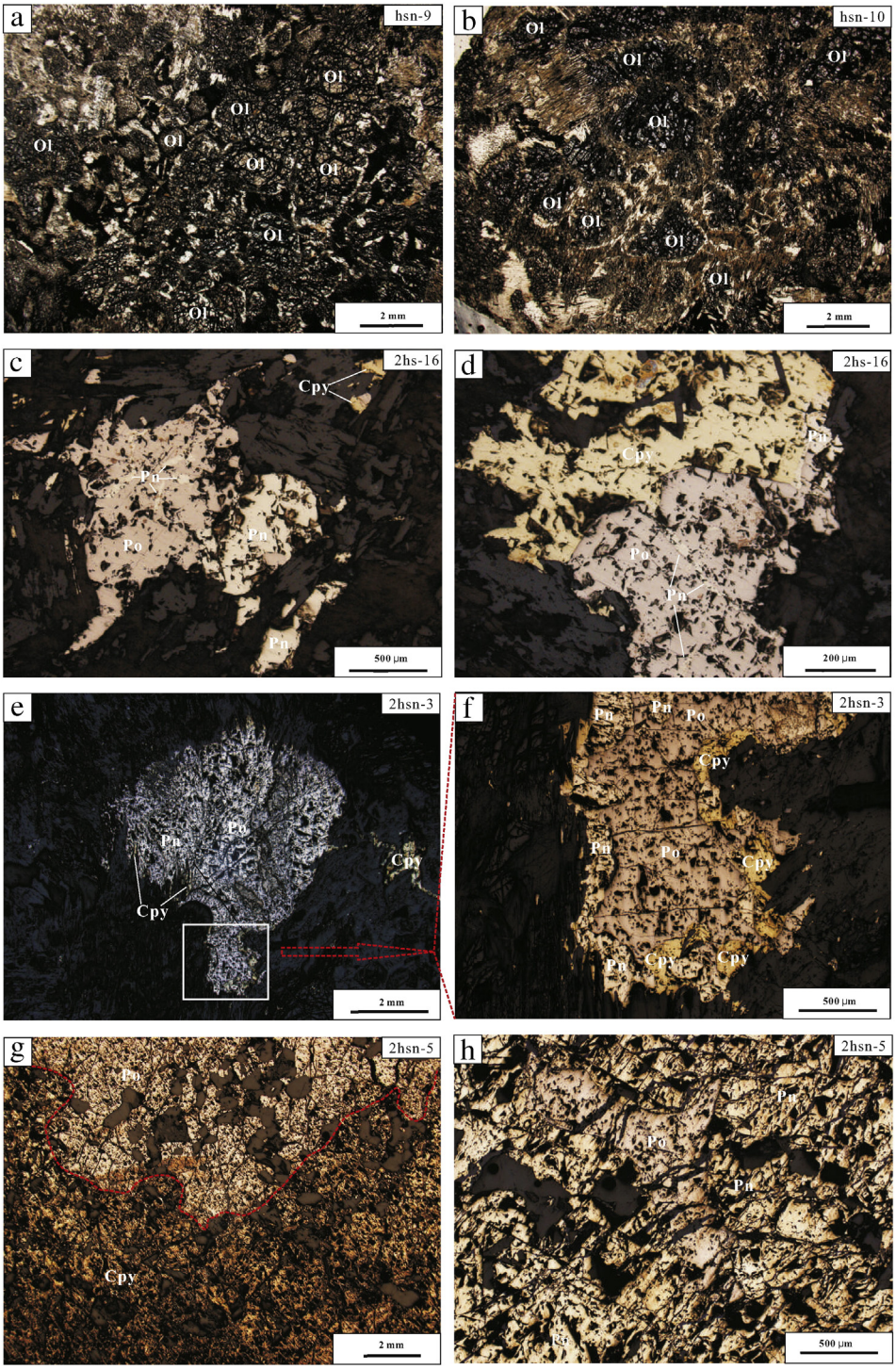


**Fig. 3.** (a) and (b) Olivinite inclusions occurring in lherzolite. (c) and (d) Sulfide minerals occurring in interstitial spaces of silicate cumulates in websterite. (e) Sulfide minerals occurring as large patches in lherzolite and (f) their coexisting relationships. (g) Massive sulfides fractionated into chalcopyrite-rich and pyrrhotite-rich zones. (h) Pyrrhotite occurring as inclusions in pentlandite. Abbreviations: Ol = olivine, Cpy = chalcopyrite, Po = pyrrhotite, Pn = pentlandite.

and websterite samples were from different adits at the 650 to 750 m and the 780 to 860 m levels, respectively (Fig. 2b). In each adit, two or three samples were collected in order to representative coverage of the mineralized part of the Huangshannan Intrusion. The samples selected for this study are unmineralized lherzolite, disseminated sulfide mineralization in the lherzolite and websterite, and massive sulfides hosted in the websterite.

### 5.1. Analysis of olivine compositions

The olivine compositions of all samples were determined in the Chinese Academy of Geological Sciences. Petrographic examination of the samples was conducted using a standard optical microscope, followed by detailed back-scattered electron imagery using a JXA-8100 electron microprobe. The major element and Ni contents were analyzed by the

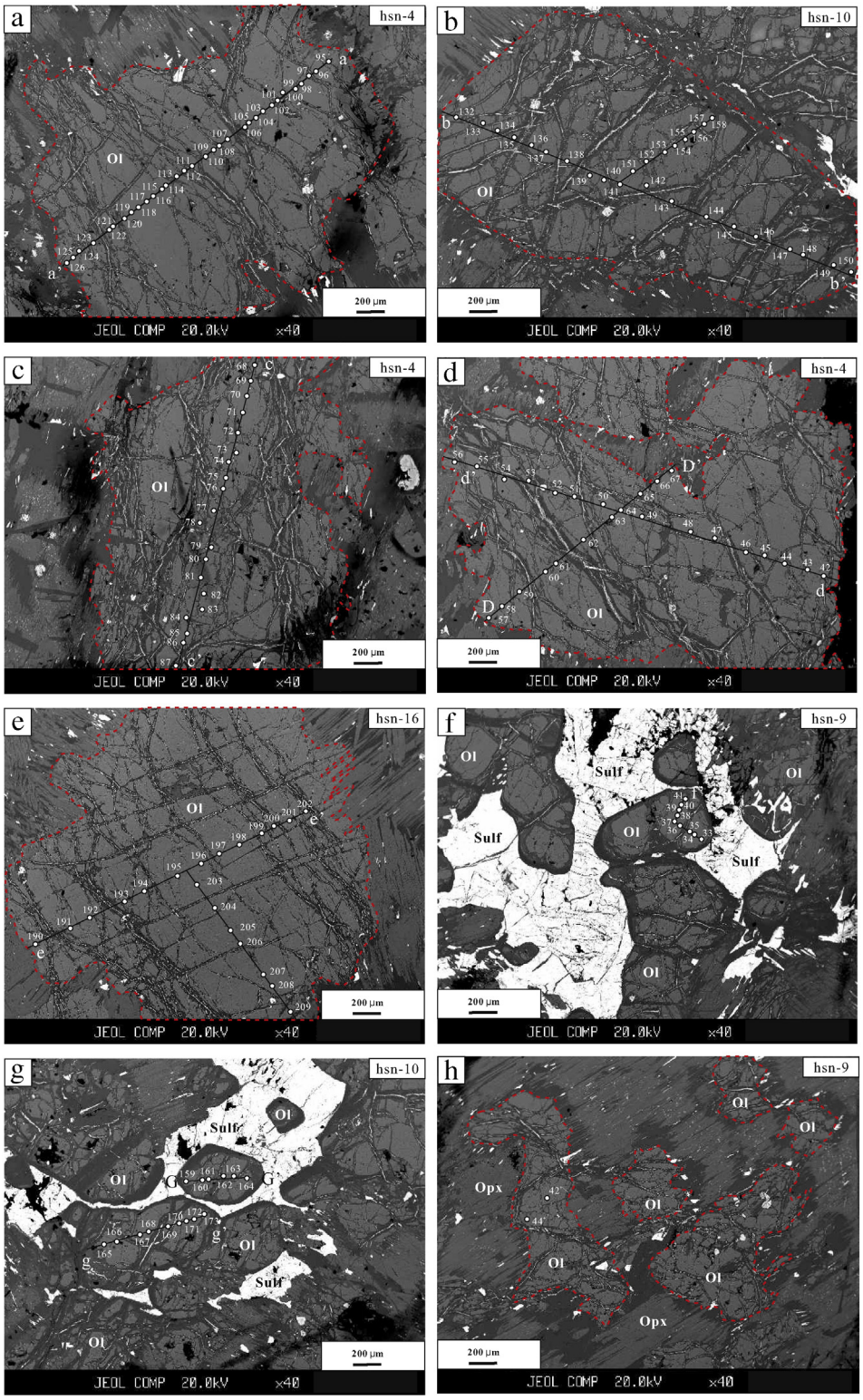


**Fig. 4.** Back-scattered electron (BSE) images showing representative textures of olivine crystals in lherzolite from the Huangshannan Intrusion. (a), (b), (c), (d) and (e) show poikilitic olivine grains. (f) and (g) show euhedral olivine grains in sulfide, and (h) shows olivine inclusion in orthopyroxene. Abbreviations: Ol = olivine, Opx = orthopyroxene, Sulf = sulfide.

electron microprobe. An accelerating voltage of 15 kV was used. Beam current and counting time for elements were 20 nA and 20 s, respectively. The detection limit for Ni under these conditions was about 250 ppm. The accuracy of analyses was monitored using an olivine standard (SPI C050-14 Serial CA AS126). Sample reproducibility varied by less than 2% relative.

### *5.2. Analysis of Ni, Cu, PGE and S contents of whole-rock samples*

Whole-rock samples were analyzed for Ni, Cu, PGE and S contents at the National Research Center of Geoanalysis in Beijing, China. Samples were powdered in an agate mortar for analysis. Whole-rock Cu and Ni contents were determined by acid digestion in steel-jacketed Teflon

**Table 1**
The olivine compositions of the lherzolite from the Huangshannan Intrusion.

| Spot no. | Type of olivine | Olivine composition (wt.%) | | | | | | | Fo (mol.%) | Ni (ppm) |
|---|---|---|---|---|---|---|---|---|---|---|
| | | $SiO_2$ | MgO | MnO | CaO | FeO | NiO | Total | | |
| *Sample no. hsn-12 unmineralized* | | | | | | | | | | |
| 2 | Core of olivine inclusion | 39.08 | 42.60 | 0.21 | nd | 17.66 | 0.494 | 100.08 | 81.13 | 3882 |
| 3 | Rim of olivine inclusion | 39.23 | 42.72 | 0.24 | 0.01 | 16.68 | 0.448 | 99.40 | 82.04 | 3520 |
| 4 | Rim of olivine inclusion | 39.23 | 42.18 | 0.22 | 0.01 | 16.96 | 0.480 | 99.10 | 81.60 | 3772 |
| 5 | Core of olivine inclusion | 38.72 | 42.66 | 0.20 | 0.02 | 17.80 | 0.380 | 99.80 | 81.03 | 2986 |
| 6 | Rim of olivine inclusion | 38.61 | 41.66 | 0.21 | nd | 18.19 | 0.360 | 99.04 | 80.33 | 2829 |
| 7 | Core of olivine inclusion | 39.36 | 43.60 | 0.17 | nd | 15.53 | 0.383 | 99.10 | 83.34 | 3010 |
| 8 | Rim of olivine inclusion | 38.85 | 42.06 | 0.21 | 0.03 | 17.94 | 0.283 | 99.42 | 80.69 | 2224 |
| *Sample no. hsn-3 disseminated sulfide mineralization* | | | | | | | | | | |
| 9 | Core of olivine inclusion | 39.01 | 43.53 | 0.20 | 0.01 | 15.92 | 0.432 | 99.21 | 82.98 | 3395 |
| 10 | Rim of olivine inclusion | 39.51 | 43.61 | 0.16 | nd | 15.49 | 0.412 | 99.36 | 83.39 | 3238 |
| 11 | Core of olivine inclusion | 39.66 | 43.14 | 0.21 | nd | 16.14 | 0.412 | 99.64 | 82.65 | 3238 |
| 12 | Core of olivine inclusion | 39.46 | 44.85 | 0.20 | nd | 14.47 | 0.394 | 99.56 | 84.68 | 3096 |
| 13 | Rim of olivine inclusion | 38.86 | 36.17 | 0.19 | 2.41 | 15.26 | 0.367 | 99.20 | 80.86 | 2884 |
| 14 | Core of olivine inclusion | 39.07 | 42.29 | 0.21 | 0.02 | 17.25 | 0.438 | 99.47 | 81.38 | 3442 |
| 15 | Rim of olivine inclusion | 39.31 | 42.42 | 0.19 | nd | 17.90 | 0.387 | 100.31 | 80.85 | 3041 |
| 16 | Core of olivine inclusion | 38.73 | 42.00 | 0.22 | 0.02 | 18.16 | 0.421 | 99.60 | 80.48 | 3308 |
| 17 | Rim of olivine inclusion | 38.76 | 42.26 | 0.20 | nd | 18.17 | 0.401 | 99.93 | 80.56 | 3151 |
| *Sample no. hsn-13 disseminated sulfide mineralization* | | | | | | | | | | |
| 18 | Core of olivine inclusion | 38.52 | 43.28 | 0.20 | nd | 16.66 | 0.293 | 98.96 | 82.24 | 2302 |
| 19 | Core of olivine inclusion | 39.31 | 42.93 | 0.20 | nd | 17.28 | 0.411 | 100.18 | 81.58 | 3230 |
| 20 | Rim of olivine inclusion | 39.43 | 43.37 | 0.19 | nd | 16.00 | 0.358 | 99.36 | 82.86 | 2813 |
| 21 | Core of olivine inclusion | 39.18 | 43.15 | 0.17 | nd | 16.83 | 0.416 | 99.78 | 82.04 | 3269 |
| 22 | Rim of olivine inclusion | 39.31 | 42.92 | 0.19 | 0.04 | 16.57 | 0.512 | 99.62 | 82.20 | 4023 |
| 23 | Core of olivine inclusion | 38.91 | 42.86 | 0.24 | 0.02 | 17.82 | 0.427 | 100.29 | 81.09 | 3355 |
| 24 | Core of olivine inclusion | 38.82 | 42.36 | 0.25 | nd | 17.40 | 0.411 | 99.25 | 81.27 | 3230 |
| 25 | Rim of olivine inclusion | 38.66 | 43.38 | 0.21 | nd | 17.48 | 0.260 | 100.26 | 81.56 | 2043 |
| *Sample no. hsn-9 disseminated sulfide mineralization* | | | | | | | | | | |
| 33 | Olivine grain in sulfide | 39.73 | 43.11 | 0.18 | nd | 16.94 | 0.294 | 100.41 | 81.94 | 2310 |
| 34 | Olivine grain in sulfide | 39.77 | 42.78 | 0.21 | nd | 16.86 | 0.303 | 100.01 | 81.89 | 2381 |
| 35 | Olivine grain in sulfide | 39.96 | 42.59 | 0.24 | 0.02 | 17.11 | 0.244 | 100.18 | 81.60 | 1917 |
| 36 | Olivine grain in sulfide | 39.39 | 42.74 | 0.17 | nd | 17.17 | 0.201 | 99.72 | 81.61 | 1579 |
| 37 | Olivine grain in sulfide | 39.57 | 42.63 | 0.17 | 0.01 | 17.17 | 0.294 | 99.85 | 81.57 | 2310 |
| 38 | Olivine grain in sulfide | 39.72 | 42.64 | 0.21 | 0.01 | 16.94 | 0.324 | 99.87 | 81.77 | 2546 |
| 39 | Olivine grain in sulfide | 39.68 | 42.77 | 0.22 | nd | 17.00 | 0.274 | 99.99 | 81.77 | 2153 |
| 40 | Olivine grain in sulfide | 39.71 | 43.06 | 0.22 | nd | 16.94 | 0.330 | 100.29 | 81.92 | 2593 |
| 41 | Olivine grain in sulfide | 39.64 | 42.79 | 0.19 | nd | 16.94 | 0.301 | 99.94 | 81.83 | 2365 |
| 42+ | Core of olivine inclusion | 39.39 | 42.26 | 0.22 | nd | 17.17 | 0.382 | 99.46 | 81.43 | 3002 |
| 44+ | Rim of olivine inclusion | 39.84 | 42.58 | 0.26 | nd | 16.94 | 0.263 | 99.93 | 81.75 | 2067 |
| *Sample no. hsn-4 disseminated sulfide mineralization* | | | | | | | | | | |
| 42 | Poikilitic crystal | 38.80 | 42.01 | 0.21 | nd | 18.49 | 0.413 | 99.95 | 80.19 | 3245 |
| 43 | Poikilitic crystal | 39.01 | 42.96 | 0.21 | nd | 17.12 | 0.410 | 99.77 | 81.73 | 3222 |
| 44 | Poikilitic crystal | 39.43 | 43.30 | 0.21 | nd | 15.64 | 0.432 | 99.06 | 83.15 | 3395 |
| 45 | Poikilitic crystal | 39.02 | 43.25 | 0.25 | nd | 16.77 | 0.359 | 99.74 | 82.13 | 2821 |
| 46 | Poikilitic crystal | 39.28 | 42.55 | 0.18 | 0.03 | 17.29 | 0.401 | 99.82 | 81.43 | 3151 |
| 47 | Poikilitic crystal | 38.94 | 42.46 | 0.16 | nd | 18.09 | 0.390 | 100.06 | 80.71 | 3065 |
| 48 | Poikilitic crystal | 39.07 | 41.60 | 0.23 | nd | 17.73 | 0.400 | 99.07 | 80.70 | 3143 |
| 49 | Poikilitic crystal | 39.03 | 40.88 | 0.21 | 0.11 | 18.75 | 0.320 | 99.41 | 79.54 | 2515 |
| 50 | Poikilitic crystal | 39.01 | 41.68 | 0.22 | 0.01 | 17.63 | 0.422 | 99.03 | 80.83 | 3316 |
| 51 | Poikilitic crystal | 38.57 | 41.75 | 0.21 | nd | 18.44 | 0.425 | 99.43 | 80.14 | 3340 |
| 52 | Poikilitic crystal | 38.65 | 41.60 | 0.24 | nd | 18.91 | 0.389 | 100.20 | 79.68 | 3057 |
| 53 | Poikilitic crystal | 39.21 | 41.71 | 0.22 | nd | 18.51 | 0.277 | 99.95 | 80.07 | 2177 |
| 54 | Poikilitic crystal | 38.97 | 41.75 | 0.22 | nd | 17.80 | 0.368 | 99.13 | 80.69 | 2892 |
| 56 | Poikilitic crystal | 38.89 | 41.27 | 0.24 | nd | 18.36 | 0.300 | 99.10 | 80.03 | 2357 |
| 57 | Poikilitic crystal | 38.83 | 41.18 | 0.20 | 0.05 | 18.53 | 0.353 | 99.18 | 79.84 | 2774 |
| 58 | Poikilitic crystal | 38.77 | 40.85 | 0.20 | 0.05 | 19.40 | 0.435 | 99.79 | 78.97 | 3418 |
| 59 | Poikilitic crystal | 41.02 | 39.21 | 0.21 | 1.22 | 16.91 | 0.286 | 99.75 | 80.52 | 2247 |
| 60 | Poikilitic crystal | 38.55 | 41.53 | 0.24 | 0.02 | 19.13 | 0.415 | 100.11 | 79.46 | 3261 |
| 61 | Poikilitic crystal | 38.57 | 41.81 | 0.20 | 0.03 | 19.16 | 0.385 | 100.18 | 79.55 | 3025 |
| 62 | Poikilitic crystal | 38.89 | 41.59 | 0.20 | 0.01 | 18.03 | 0.466 | 99.22 | 80.43 | 3662 |
| 63 | Poikilitic crystal | 38.59 | 41.48 | 0.22 | nd | 18.74 | 0.370 | 99.42 | 79.78 | 2907 |
| 64 | Poikilitic crystal | 38.95 | 41.43 | 0.20 | nd | 19.20 | 0.283 | 100.11 | 79.37 | 2224 |
| 65 | Poikilitic crystal | 38.76 | 41.66 | 0.18 | nd | 19.36 | 0.283 | 100.28 | 79.32 | 2224 |
| 66 | Poikilitic crystal | 38.82 | 41.49 | 0.18 | nd | 18.51 | 0.300 | 99.33 | 79.98 | 2357 |
| 67 | Poikilitic crystal | 38.58 | 40.96 | 0.22 | nd | 19.19 | 0.289 | 99.29 | 79.19 | 2271 |
| 68 | Poikilitic crystal | 39.63 | 42.00 | 0.20 | nd | 17.68 | 0.345 | 99.89 | 80.90 | 2711 |
| 69 | Poikilitic crystal | 39.00 | 41.23 | 0.21 | 0.02 | 19.06 | 0.312 | 99.89 | 79.40 | 2452 |
| 70 | Poikilitic crystal | 39.28 | 41.98 | 0.16 | 0.02 | 17.48 | 0.363 | 99.37 | 81.06 | 2852 |
| 71 | Poikilitic crystal | 38.87 | 42.79 | 0.18 | nd | 17.40 | 0.322 | 99.68 | 81.42 | 2530 |
| 72 | Poikilitic crystal | 39.00 | 43.29 | 0.25 | nd | 16.52 | 0.382 | 99.52 | 82.36 | 3002 |

*(continued on next page)*

**Table 1** (*continued*)

| Spot no. | Type of olivine | Olivine composition (wt.%) | | | | | | | Fo (mol.%) | Ni (ppm) |
|---|---|---|---|---|---|---|---|---|---|---|
| | | $SiO_2$ | MgO | MnO | CaO | FeO | NiO | Total | | |
| *Sample no. hsn-4 disseminated sulfide mineralization* | | | | | | | | | | |
| 73 | Poikilitic crystal | 38.87 | 43.57 | 0.21 | 0.03 | 16.04 | 0.318 | 99.04 | 82.88 | 2499 |
| 74 | Poikilitic crystal | 39.68 | 43.31 | 0.16 | 0.03 | 15.78 | 0.396 | 99.44 | 83.03 | 3112 |
| 75 | Poikilitic crystal | 38.97 | 43.77 | 0.18 | 0.02 | 15.80 | 0.301 | 99.07 | 83.16 | 2365 |
| 76 | Poikilitic crystal | 39.13 | 44.03 | 0.23 | 0.01 | 15.72 | 0.414 | 99.61 | 83.31 | 3253 |
| 77 | Poikilitic crystal | 39.88 | 43.55 | 0.16 | nd | 15.54 | 0.366 | 99.52 | 83.32 | 2876 |
| 78 | Poikilitic crystal | 39.89 | 43.34 | 0.22 | nd | 15.76 | 0.410 | 99.64 | 83.06 | 3222 |
| 79 | Poikilitic crystal | 39.66 | 43.34 | 0.18 | 0.02 | 15.73 | 0.352 | 99.29 | 83.08 | 2766 |
| 80 | Poikilitic crystal | 39.56 | 42.97 | 0.17 | 0.05 | 16.86 | 0.357 | 100.10 | 81.96 | 2805 |
| 82 | Poikilitic crystal | 38.64 | 43.23 | 0.19 | 0.01 | 16.76 | 0.438 | 99.32 | 82.14 | 3442 |
| 83 | Poikilitic crystal | 39.97 | 42.91 | 0.18 | 0.01 | 16.15 | 0.398 | 99.64 | 82.57 | 3128 |
| 84 | Poikilitic crystal | 39.78 | 42.75 | 0.19 | nd | 16.41 | 0.409 | 99.57 | 82.28 | 3214 |
| 85 | Poikilitic crystal | 39.40 | 42.53 | 0.21 | nd | 17.67 | 0.416 | 100.26 | 81.09 | 3269 |
| 86 | Poikilitic crystal | 39.43 | 42.67 | 0.26 | nd | 17.60 | 0.417 | 100.58 | 81.21 | 3277 |
| 87 | Poikilitic crystal | 37.47 | 39.47 | 0.18 | nd | 17.46 | 0.407 | 95.09 | 80.12 | 3198 |
| 95 | Poikilitic crystal | 39.24 | 41.67 | 0.19 | 0.02 | 18.24 | 0.269 | 99.66 | 80.28 | 2114 |
| 96 | Poikilitic crystal | 38.90 | 41.61 | 0.18 | 0.02 | 18.40 | 0.351 | 99.56 | 80.12 | 2758 |
| 97 | Poikilitic crystal | 39.12 | 41.67 | 0.24 | nd | 18.17 | 0.282 | 99.48 | 80.34 | 2216 |
| 98 | Poikilitic crystal | 39.40 | 41.88 | 0.23 | 0.04 | 18.13 | 0.350 | 100.04 | 80.46 | 2750 |
| 99 | Poikilitic crystal | 39.79 | 42.32 | 0.24 | nd | 17.99 | 0.344 | 100.80 | 80.74 | 2703 |
| 100 | Poikilitic crystal | 38.68 | 41.55 | 0.21 | 0.06 | 18.91 | 0.418 | 99.97 | 79.66 | 3285 |
| 101 | Poikilitic crystal | 39.00 | 41.17 | 0.24 | 0.04 | 18.20 | 0.259 | 99.39 | 80.13 | 2035 |
| 102 | Poikilitic crystal | 39.25 | 42.37 | 0.18 | 0.03 | 17.42 | 0.414 | 99.68 | 81.26 | 3253 |
| 103 | Poikilitic crystal | 39.51 | 42.31 | 0.22 | nd | 17.15 | 0.452 | 99.69 | 81.48 | 3552 |
| 104 | Poikilitic crystal | 38.61 | 41.72 | 0.21 | nd | 17.18 | 0.397 | 99.26 | 81.24 | 3120 |
| 105 | Poikilitic crystal | 39.68 | 42.58 | 0.20 | nd | 16.47 | 0.394 | 99.34 | 82.17 | 3096 |
| 106 | Poikilitic crystal | 39.62 | 42.99 | 0.24 | 0.02 | 16.81 | 0.412 | 100.13 | 82.01 | 3238 |
| 107 | Poikilitic crystal | 39.07 | 41.84 | 0.20 | 0.03 | 16.97 | 0.346 | 99.00 | 81.46 | 2719 |
| 108 | Poikilitic crystal | 39.39 | 42.56 | 0.17 | nd | 17.45 | 0.367 | 100.06 | 81.30 | 2884 |
| 109 | Poikilitic crystal | 39.68 | 43.33 | 0.19 | nd | 15.52 | 0.411 | 99.18 | 83.26 | 3230 |
| 110 | Poikilitic crystal | 39.42 | 43.60 | 0.24 | 0.01 | 16.29 | 0.396 | 99.99 | 82.67 | 3112 |
| 111 | Poikilitic crystal | 39.27 | 43.43 | 0.20 | nd | 16.68 | 0.392 | 99.99 | 82.27 | 3080 |
| 112 | Poikilitic crystal | 39.72 | 43.79 | 0.18 | 0.01 | 16.12 | 0.393 | 100.24 | 82.88 | 3088 |
| 113 | Poikilitic crystal | 39.58 | 43.94 | 0.16 | 0.01 | 15.44 | 0.374 | 99.52 | 83.53 | 2939 |
| 114 | Poikilitic crystal | 39.77 | 44.28 | 0.19 | 0.03 | 15.58 | 0.391 | 100.28 | 83.51 | 3073 |
| 115 | Poikilitic crystal | 39.63 | 44.05 | 0.15 | 0.03 | 15.95 | 0.328 | 100.29 | 83.12 | 2577 |
| 116 | Poikilitic crystal | 39.05 | 43.03 | 0.19 | 0.25 | 16.00 | 0.338 | 99.33 | 82.74 | 2656 |
| 117 | Poikilitic crystal | 39.70 | 44.03 | 0.19 | nd | 14.93 | 0.396 | 99.26 | 84.02 | 3112 |
| 118 | Poikilitic crystal | 39.45 | 43.55 | 0.18 | 0.02 | 16.38 | 0.415 | 99.99 | 82.58 | 3261 |
| 119 | Poikilitic crystal | 39.73 | 43.24 | 0.18 | 0.02 | 16.79 | 0.304 | 100.34 | 82.11 | 2389 |
| 120 | Poikilitic crystal | 39.47 | 42.56 | 0.19 | 0.04 | 17.57 | 0.405 | 100.28 | 81.20 | 3183 |
| 121 | Poikilitic crystal | 39.22 | 41.98 | 0.23 | 0.01 | 17.89 | 0.353 | 99.69 | 80.70 | 2774 |
| 122 | Poikilitic crystal | 39.33 | 42.08 | 0.20 | 0.04 | 17.04 | 0.415 | 99.21 | 81.49 | 3261 |
| 123 | Poikilitic crystal | 38.70 | 41.20 | 0.20 | 0.06 | 18.76 | 0.387 | 99.67 | 79.65 | 3041 |
| 124 | Poikilitic crystal | 39.02 | 41.21 | 0.18 | 0.06 | 19.24 | 0.248 | 99.95 | 79.25 | 1949 |
| 125 | Poikilitic crystal | 39.24 | 41.40 | 0.25 | nd | 18.53 | 0.252 | 99.67 | 79.93 | 1980 |
| 126 | Poikilitic crystal | 40.02 | 40.11 | 0.25 | 0.58 | 18.22 | 0.289 | 100.20 | 79.69 | 2271 |
| *Sample no. hsn-10 disseminated sulfide mineralization* | | | | | | | | | | |
| 130 | Core of olivine inclusion | 39.41 | 43.68 | 0.17 | nd | 16.50 | 0.368 | 100.19 | 82.51 | 2892 |
| 131 | Rim of olivine inclusion | 39.37 | 43.50 | 0.23 | nd | 16.38 | 0.431 | 100.02 | 82.56 | 3387 |
| 132 | Poikilitic crystal | 39.56 | 44.65 | 0.24 | nd | 14.77 | 0.196 | 99.46 | 84.35 | 1540 |
| 133 | Poikilitic crystal | 39.60 | 43.55 | 0.22 | nd | 15.40 | 0.386 | 99.24 | 83.45 | 3033 |
| 134 | Poikilitic crystal | 40.07 | 43.67 | 0.23 | 0.02 | 14.96 | 0.456 | 99.43 | 83.88 | 3583 |
| 135 | Poikilitic crystal | 39.69 | 43.87 | 0.21 | 0.02 | 14.87 | 0.477 | 99.25 | 84.02 | 3748 |
| 136 | Poikilitic crystal | 40.01 | 44.62 | 0.18 | nd | 14.72 | 0.370 | 99.95 | 84.38 | 2907 |
| 137 | Poikilitic crystal | 40.03 | 44.41 | 0.19 | nd | 14.37 | 0.423 | 99.47 | 84.64 | 3324 |
| 138 | Poikilitic crystal | 39.75 | 44.31 | 0.18 | nd | 15.41 | 0.397 | 100.25 | 83.68 | 3120 |
| 139 | Poikilitic crystal | 39.97 | 44.90 | 0.15 | 0.02 | 14.29 | 0.403 | 99.74 | 84.85 | 3167 |
| 140 | Poikilitic crystal | 39.90 | 44.89 | 0.19 | nd | 14.20 | 0.350 | 99.57 | 84.92 | 2750 |
| 141 | Poikilitic crystal | 39.87 | 44.59 | 0.18 | nd | 15.05 | 0.370 | 100.09 | 84.08 | 2907 |
| 142 | Poikilitic crystal | 39.15 | 44.17 | 0.18 | nd | 15.04 | 0.392 | 99.22 | 83.96 | 3080 |
| 143 | Poikilitic crystal | 40.02 | 44.50 | 0.17 | 0.01 | 14.59 | 0.396 | 99.71 | 84.46 | 3112 |
| 144 | Poikilitic crystal | 40.14 | 44.46 | 0.18 | nd | 15.00 | 0.404 | 100.32 | 84.08 | 3175 |
| 145 | Poikilitic crystal | 39.78 | 44.33 | 0.22 | 0.04 | 14.66 | 0.453 | 99.55 | 84.35 | 3560 |
| 146 | Poikilitic crystal | 39.68 | 43.96 | 0.16 | nd | 15.81 | 0.363 | 100.06 | 83.21 | 2852 |
| 147 | Poikilitic crystal | 39.19 | 43.93 | 0.19 | nd | 15.41 | 0.397 | 99.19 | 83.56 | 3120 |
| 148 | Poikilitic crystal | 39.32 | 44.00 | 0.18 | nd | 16.18 | 0.363 | 100.05 | 82.90 | 2852 |
| 149 | Poikilitic crystal | 39.36 | 44.29 | 0.18 | nd | 15.29 | 0.287 | 99.45 | 83.78 | 2255 |
| 150 | Poikilitic crystal | 39.85 | 45.02 | 0.17 | nd | 15.03 | 0.304 | 100.40 | 84.23 | 2389 |
| 151 | Poikilitic crystal | 39.55 | 44.73 | 0.15 | nd | 15.12 | 0.387 | 99.96 | 84.06 | 3041 |
| 152 | Poikilitic crystal | 39.71 | 44.99 | 0.15 | nd | 14.89 | 0.402 | 100.17 | 84.34 | 3159 |
| 153 | Poikilitic crystal | 40.43 | 43.78 | 0.19 | 0.99 | 14.32 | 0.246 | 100.08 | 84.49 | 1933 |
| 154 | Poikilitic crystal | 39.64 | 44.63 | 0.19 | 0.02 | 14.54 | 0.480 | 99.54 | 84.55 | 3772 |
| 155 | Poikilitic crystal | 39.70 | 44.30 | 0.23 | nd | 15.52 | 0.382 | 100.19 | 83.57 | 3002 |

**Table 1** (*continued*)

| Spot no. | Type of olivine | Olivine composition (wt.%) | | | | | | | Fo (mol.%) | Ni (ppm) |
|---|---|---|---|---|---|---|---|---|---|---|
| | | $SiO_2$ | MgO | MnO | CaO | FeO | NiO | Total | | |
| *Sample no. hsn-10 disseminated sulfide mineralization* | | | | | | | | | | |
| 156 | Poikilitic crystal | 39.66 | 43.74 | 0.22 | 0.03 | 16.03 | 0.393 | 100.10 | 82.95 | 3088 |
| 157 | Poikilitic crystal | 39.57 | 43.94 | 0.17 | 0.01 | 16.00 | 0.365 | 100.10 | 83.03 | 2868 |
| 158 | Poikilitic crystal | 39.51 | 43.92 | 0.21 | 0.02 | 15.85 | 0.341 | 99.90 | 83.16 | 2680 |
| 159 | Olivine grain in sulfide | 40.09 | 44.84 | 0.21 | nd | 14.34 | 0.287 | 99.82 | 84.79 | 2255 |
| 160 | Olivine grain in sulfide | 39.63 | 44.61 | 0.21 | nd | 14.56 | 0.289 | 99.33 | 84.53 | 2271 |
| 161 | Olivine grain in sulfide | 39.10 | 43.81 | 0.22 | nd | 15.26 | 0.393 | 99.01 | 83.66 | 3088 |
| 162 | Olivine grain in sulfide | 39.66 | 44.43 | 0.14 | nd | 14.67 | 0.311 | 99.26 | 84.38 | 2444 |
| 163 | Olivine grain in sulfide | 39.73 | 44.60 | 0.22 | nd | 15.06 | 0.364 | 99.98 | 84.08 | 2860 |
| 164 | Olivine grain in sulfide | 39.40 | 44.42 | 0.23 | nd | 15.21 | 0.310 | 99.60 | 83.89 | 2436 |
| 165 | Olivine grain in sulfide | 39.76 | 44.04 | 0.16 | nd | 15.05 | 0.415 | 99.49 | 83.91 | 3261 |
| 166 | Olivine grain in sulfide | 39.24 | 44.12 | 0.21 | nd | 16.13 | 0.374 | 100.11 | 82.98 | 2939 |
| 167 | Olivine grain in sulfide | 39.87 | 44.23 | 0.18 | nd | 14.73 | 0.476 | 99.55 | 84.26 | 3740 |
| 168 | Olivine grain in sulfide | 39.68 | 44.10 | 0.21 | 0.01 | 15.68 | 0.464 | 100.17 | 83.37 | 3646 |
| 169 | Olivine grain in sulfide | 39.15 | 43.72 | 0.26 | nd | 16.08 | 0.439 | 99.73 | 82.90 | 3450 |
| 170 | Olivine grain in sulfide | 39.55 | 44.06 | 0.22 | 0.01 | 16.00 | 0.345 | 100.20 | 83.08 | 2711 |
| 171 | Olivine grain in sulfide | 39.42 | 43.89 | 0.24 | 0.01 | 15.67 | 0.355 | 99.63 | 83.31 | 2790 |
| 172 | Olivine grain in sulfide | 39.85 | 44.57 | 0.23 | 0.01 | 14.43 | 0.364 | 99.50 | 84.62 | 2860 |
| 173 | Olivine grain in sulfide | 39.41 | 44.06 | 0.21 | 0.01 | 15.19 | 0.269 | 99.22 | 83.80 | 2114 |
| *Sample no. hsn-16 disseminated sulfide mineralization* | | | | | | | | | | |
| 191 | Poikilitic crystal | 39.25 | 42.73 | 0.20 | nd | 16.61 | 0.352 | 99.15 | 82.10 | 2766 |
| 192 | Poikilitic crystal | 39.42 | 43.81 | 0.18 | nd | 15.50 | 0.381 | 99.30 | 83.44 | 2994 |
| 193 | Poikilitic crystal | 39.75 | 43.74 | 0.20 | 0.69 | 14.33 | 0.405 | 99.19 | 84.47 | 3183 |
| 194 | Poikilitic crystal | 39.48 | 44.48 | 0.17 | nd | 14.84 | 0.440 | 99.43 | 84.23 | 3458 |
| 195 | Poikilitic crystal | 39.32 | 44.26 | 0.16 | nd | 14.72 | 0.405 | 99.35 | 84.27 | 3183 |
| 196 | Poikilitic crystal | 39.78 | 44.51 | 0.13 | 0.01 | 14.41 | 0.363 | 99.29 | 84.63 | 2852 |
| 197 | Poikilitic crystal | 39.41 | 44.18 | 0.18 | nd | 15.20 | 0.403 | 99.46 | 83.82 | 3167 |
| 198 | Poikilitic crystal | 39.70 | 43.87 | 0.17 | nd | 15.39 | 0.417 | 99.59 | 83.56 | 3277 |
| 199 | Poikilitic crystal | 39.31 | 43.48 | 0.16 | 0.22 | 16.23 | 0.382 | 99.89 | 82.68 | 3002 |
| 200 | Poikilitic crystal | 39.10 | 43.70 | 0.15 | nd | 15.66 | 0.410 | 99.07 | 83.26 | 3222 |
| 201 | Poikilitic crystal | 39.71 | 43.09 | 0.16 | 0.39 | 15.54 | 0.406 | 99.41 | 83.17 | 3190 |
| 202 | Poikilitic crystal | 39.48 | 42.82 | 0.17 | nd | 16.78 | 0.369 | 99.65 | 81.98 | 2900 |
| 203 | Poikilitic crystal | 39.59 | 44.80 | 0.25 | nd | 14.20 | 0.350 | 99.21 | 84.90 | 2750 |
| 204 | Poikilitic crystal | 39.44 | 45.02 | 0.19 | 0.01 | 14.76 | 0.359 | 99.81 | 84.46 | 2821 |
| 205 | Poikilitic crystal | 39.91 | 44.57 | 0.14 | nd | 15.18 | 0.380 | 100.24 | 83.96 | 2986 |
| 206 | Poikilitic crystal | 39.34 | 44.12 | 0.15 | nd | 16.04 | 0.424 | 100.07 | 83.06 | 3332 |
| 207 | Poikilitic crystal | 39.16 | 43.28 | 0.20 | 0.10 | 16.03 | 0.384 | 99.15 | 82.79 | 3018 |
| 208 | Poikilitic crystal | 38.93 | 41.90 | 0.19 | 0.01 | 18.45 | 0.278 | 99.83 | 80.19 | 2185 |
| 209 | Poikilitic crystal | 38.56 | 42.30 | 0.19 | nd | 18.89 | 0.395 | 100.37 | 79.97 | 3104 |

Notes: nd = The contents of elements are below the lower limit of detection.

"bombs", followed by inductively coupled plasma-mass spectrometry (ICP-MS) analysis. The accuracies are estimated to be better than 2 to 10% relative standard deviation (RSD). Whole-rock S contents were measured using a high-frequency infrared carbon sulfur analyzer. The detection limits are 0.005% and the accuracies are estimated to be better than 10% RSD. The contents of PGE were determined by nickel sulfide fire-assay and Te-coprecipitation, followed by ICP-MS analysis. A detailed description of the method for PGE analysis is given by Asif and Parry (1991). Precision and accuracy were established through the analysis of reference materials UMT-1 and WPR-1; both precision and accuracy for all elements determined by ICP-MS are better than 10% RSD.

## 6. Analytical results

The compositions of the various types of olivine from the Huangshannan Intrusion are reported in Table 1. Whole-rock Ni, Cu, PGE and S contents are listed in Table 2.

### 6.1. Olivine compositional variations

The poikilitic olivine is characterized by large variations in both Fo and Ni contents, ranging from 78.97 to 84.92 mol.% and from 1540 to 3772 ppm, respectively (Table 1). The cores of olivine grains are

**Table 2**
Ni, Cu, PGE and S contents of sulfide mineralization from the Huangshannan Deposit.

| Mineralization type | Disseminated sulfide mineralization in websterite | | | | | | | Massive sulfide | | | | | |
|---|---|---|---|---|---|---|---|---|---|---|---|---|---|
| Sample no. | 2hs-2 | 2hs-3 | 2hs-7 | 2hs-8 | 2hs-11 | 2hs-12 | 2hs-16 | 2hs-1 | 2hs-20 | 2hs-21 | 2hs-22 | 2hsn-5-1 | 2hsn-5-2 |
| S (wt.%) | 0.82 | 1.71 | 1.19 | 1.89 | 1.07 | 0.56 | 1.57 | 31.86 | 21.02 | 22.18 | 38.16 | 34.81 | 34.4 |
| Ni (wt.%) | 0.196 | 0.363 | 0.343 | 0.483 | 0.272 | 0.159 | 0.387 | 13.340 | 6.779 | 5.435 | 9.552 | 8.068 | 10.080 |
| Cu (wt.%) | 0.080 | 0.467 | 0.265 | 0.320 | 0.117 | 0.109 | 0.457 | 0.553 | 3.595 | 4.378 | 1.746 | 0.060 | 0.056 |
| Os (ppb) | 0.42 | 0.21 | 0.19 | 0.34 | 0.5 | 0.25 | 0.49 | 22.4 | 7.79 | 6.5 | 10.3 | 0.8 | 6.85 |
| Ir (ppb) | 0.24 | 0.12 | 0.17 | 0.19 | 0.27 | 0.14 | 0.27 | 12.8 | 5.39 | 3.56 | 5.82 | 0.51 | 3.88 |
| Ru (ppb) | 0.34 | 0.17 | 0.18 | 0.22 | 0.41 | 0.18 | 0.34 | 16.9 | 5.66 | 5.07 | 6.7 | 0.99 | 5.46 |
| Rh (ppb) | 0.19 | 0.24 | 0.18 | 0.25 | 0.26 | 0.18 | 0.48 | 10.2 | 4.17 | 4.41 | 6.03 | 4.31 | 7.12 |
| Pt (ppb) | 2.43 | 21.4 | 6.93 | 21.2 | 13.2 | 5.36 | 24.3 | 7.29 | 0.97 | 1.41 | 0.7 | 1.1 | 1.4 |
| Pd (ppb) | 4.45 | 28 | 16.8 | 26.5 | 18.7 | 7.49 | 33.4 | 132 | 75.7 | 178 | 164 | 44.4 | 110 |

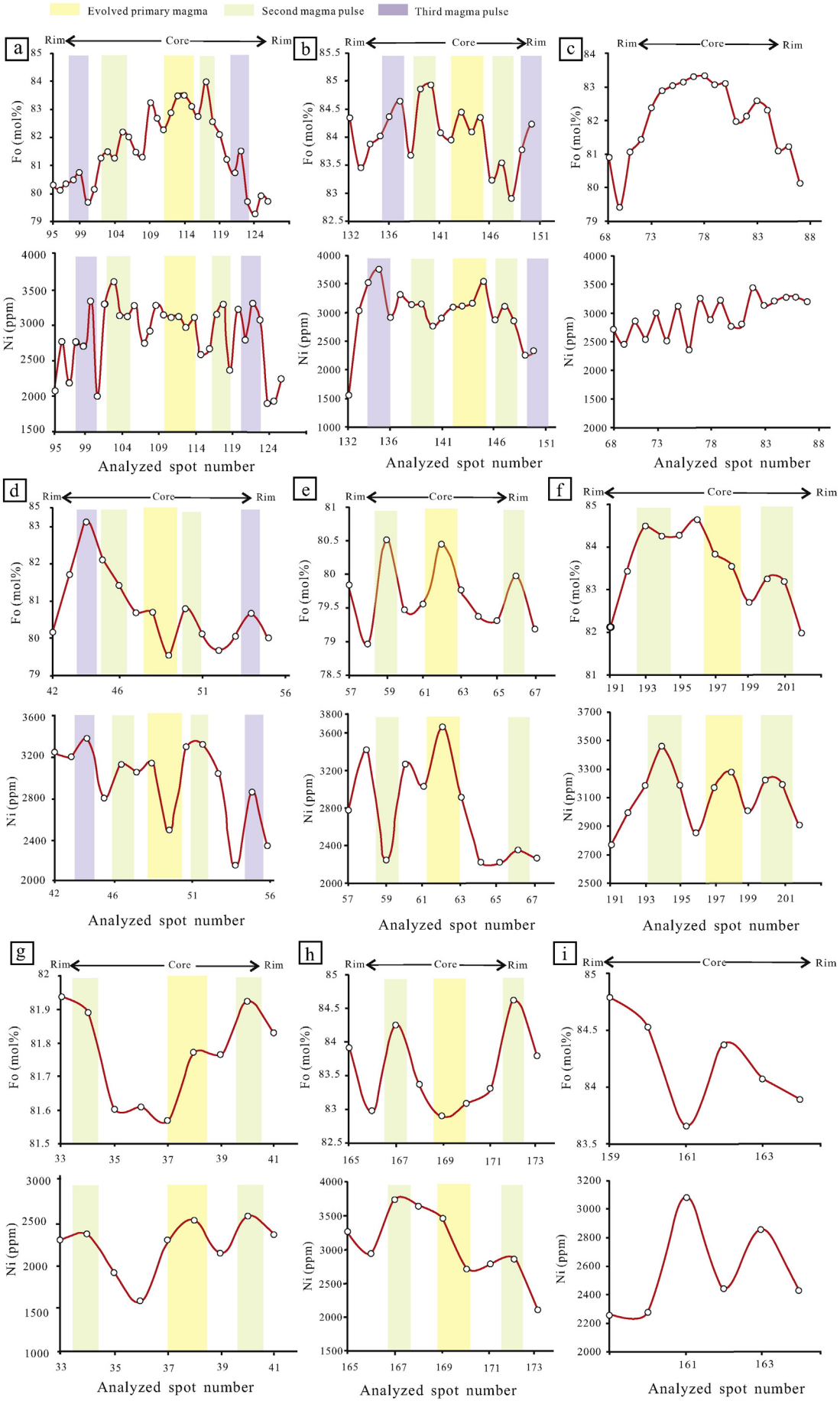
Evolved primary magma
Second magma pulse
Third magma pulse
a
b
c
d
e
f
g
h
i
Rim
Core
Rim
Fo (mol%)
Ni (ppm)
Analyzed spot number

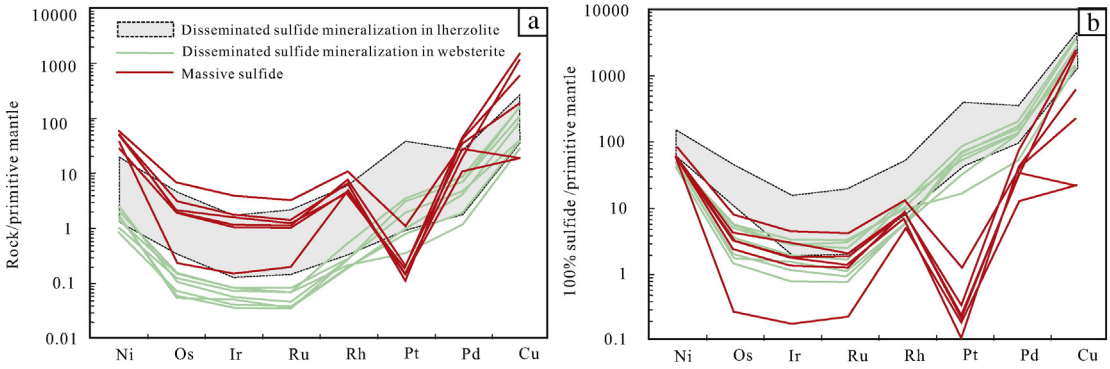


**Fig. 6.** Primitive mantle-normalized Ni, Cu and PGE patterns of the sulfide mineralization from the Huangshannan Intrusion. These elements are represented in whole-rock compositions (a) and recalculated to 100% sulfide (b), respectively. Primitive mantle values are from McDonough and Sun (1995) and Barnes and Maier (1999). Data for the lherzolite-hosted sulfide mineralization are from Zhao et al. (2015).

characterized by relatively high Fo and Ni contents, ranging from 83.15 to 84.92 mol.% and from 3442 to 3772 ppm, respectively. The rims of olivine grains have relatively low Fo and Ni contents (Fig. 5a, b, c, d, e and f), ranging from 78.97 to 82.93 mol.% and from 1540 to 2365 ppm, respectively. The olivine grains in the olivinite (Sample no. hsn-10) have the highest Fo and Ni contents of all samples analyzed in this study (Fo: 84.92 mol.% and Ni: 3772 ppm).

Olivine grains in sulfide exhibit variable Fo and Ni contents (Fig. 5g and h) (Sample no. hsn-10, Fo: 82.90–84.79 mol.% and Ni: 2114–3740 ppm; Sample no. hsn-9, Fo: 81.57–81.94 mol.% and Ni: 1579–2593 ppm). Some of the olivine grains in sulfide exhibit a negative relationship between the Ni and Fo contents (Fig. 5i).

Olivine inclusions in pyroxene oikocrysts exhibit large variations in Fo and Ni contents, ranging from 80.33 to 84.68 mol.% and from 2043 to 4023 ppm, respectively. The cores of olivine grains are characterized by higher Fo and Ni contents (Fo: 80.48–84.68 mol.% with a mean of 81.99 mol.% and Ni: 2302–3882 ppm with a mean of 3176 ppm) than the rims of olivine grains (Fo: 80.33–83.39 mol.% with a mean of 81.63 mol.% and Ni: 2043–4023 ppm with a mean of 2999 ppm).

### *6.2. Ni, Cu and PGE contents of the sulfides*

Massive sulfides have higher PGE concentrations than the disseminated sulfide mineralization (Fig. 6a). The disseminated sulfide mineralization hosted in lherzolite shows similar fractionated PGE patterns but much higher PGE contents than the disseminated sulfide mineralization in the websterite (Fig. 6a). The disseminated sulfide mineralization hosted in lherzolite is characterized by much higher PGE tenors than the disseminated sulfide mineralization in websterite and massive sulfides (Fig. 6b). Samples with sulfide mineralization show a strong positive correlation between Ir and Os, Ru and Rh, and a poor correlation between Ir and Pt or Pd (Fig. 7). The disseminated sulfide mineralization in the websterite shows slightly higher Pd/Ir and Pd/Pt ratios than the disseminated mineralization in the lherzolite (Fig. 7). The massive sulfides show much higher Pd/Pt and lower Pt/Ir ratios than disseminated mineralization due to the significantly lower Pt concentration (Figs. 6a and 7).

## 7. Discussion

### *7.1. Different magma pulses and types in the formation of the Huangshannan Intrusion*

The composition of olivine is controlled mainly by that of the parental magma, fractional crystallization, reactions with interstitial silicate and sulfide liquids, and hydrothermal alteration at elevated temperatures (Li et al., 2003, 2007; Chen et al., 2009; Deng et al., 2012). Nickel and Mg are compatible in early crystallizing olivine whereas Fe is less compatible relative to Mg. Thus, Fo and Ni contents in olivine decrease gradually from core to rim as the crystallization of olivine proceeds. However, the compositions of crystallized olivine may be modified by "trapped silicate liquid shift" (Barnes, 1986; Li et al., 2003, 2007), which generates olivine with a composition that is poorer in Mg than the original material. Poikilitic olivine crystals from the Huangshannan Intrusion may have been modified in this way, resulting in lower Fo and relatively restricted Ni contents relative to the starting composition of the olivine (Figs. 4c and 5c). When olivine is immersed in sulfide liquid, Ni and Fe may exchange between the olivine crystal and sulfide melt according to the reaction: $NiO_{olivine} + FeS_{sulfide} = NiS_{sulfide} + FeO_{olivine}$ (Li et al., 2003, 2007). This process will produce an inverse relationship between Fo and Ni contents in olivine (Li et al., 2003, 2007). Olivine grains in sulfide from the Huangshannan Intrusion may have been subjected to sub-solidus re-equilibration with trapped sulfide liquid, as reflected by the inverse relationship between Fo and Ni contents (Figs. 4f, g and 5i). Olivine grains that experienced obvious metamorphism or alteration have been avoided in this study in order to interpret the evolution history of parental magma.

Most of the olivine grains are characterized by symmetric and reproducible variations with the same trend change in Fo and Ni contents from core to margin (Fig. 5a, b, d, e, f, g and h). These symmetric and reproducible variations cannot be explained by normal olivine crystallization, by "trapped silicate liquid shift" or by Ni–Fe exchange between olivine and sulfide liquid as discussed above. During the formation of the olivine crystals, a new magma pulse with higher Mg and Ni concentrations than an evolved primary magma will result in the increase of both Fo and Ni contents. Then the Fo and Ni contents in olivine will decrease gradually as the crystallization of olivine proceeds. Another magma pulse with higher Mg and Ni concentrations than the evolved magma in the chamber may contribute to the increase of both Fo and Ni content again. In summary, the continuous equilibration of the olivine with new magma pulses resulted in the symmetric and reproducible variations in both Fo and Ni contents in olivine crystals.

The formation of the mineralized Huangshannan Intrusion may be modeled by the PGE tenors of the sulfide mineralization, using the mass-balance R-factor (mass ratio for silicate- to sulfide-melts) equation (Campbell and Naldrett, 1979) and Rayleigh equation. Numerical modeling is carried out using the sulfide/magma partition coefficients of 20,000 for Pd, 30,000 for Ir, and 30,000 for Os, and the MSS/sulfide liquid partition coefficients of 0.1 for Pd, 3.5 for Ir, and 3.5 for Os. These

**Fig. 5.** Compositional traverses across olivine crystals occurring in the lherzolite. The locations of the traverses and analyzed spot number correspond to those shown in Fig. 4. (a), (b), (d), (e), (f), (g) and (h) show symmetric and reproducible variations of Fo and Ni contents from the core to the rim. (c) shows that the Fo content of olivine decreases from the core to the rim whereas the Ni content shows relatively restricted range, and (i) shows that some of olivine grains in magmatic sulfides exhibit a negative relationship between the Fo and Ni contents.

partition coefficients are within the ranges of experimental results (see summary in Barnes and Lightfoot, 2005). The mass-balance modeling shows that the parental magma of lherzolite contains 0.04 ppb Os, 0.02 ppb Ir and 0.4 ppb Pd with R factors ranging from 1000 to 5000 (Fig. 8). The parental magma that formed websterite is calculated to have 0.02 ppb Os, 0.009 ppb Ir and 0.75 ppb Pd with R factors from 500 to 1000 (Fig. 8). The different compositions of the parental magmas indicate that they were generated from different sources or have different contributions of mantle versus crustal material (e.g., Zhao et al., 2015). The massive sulfides show a positive correlation between Ir and Os, Ru or Rh, and no obvious correlations between Ir and Pt or Pd (Fig. 7), which may be due to the crystallization and removal of MSS from sulfide melts during cooling. We used the Rayleigh equation to simulate the fractionation of the sulfide melts. Our calculations show that the formation of the massive sulfides can be explained by MSS-sulfide liquid fractionation from the same magma pulse that

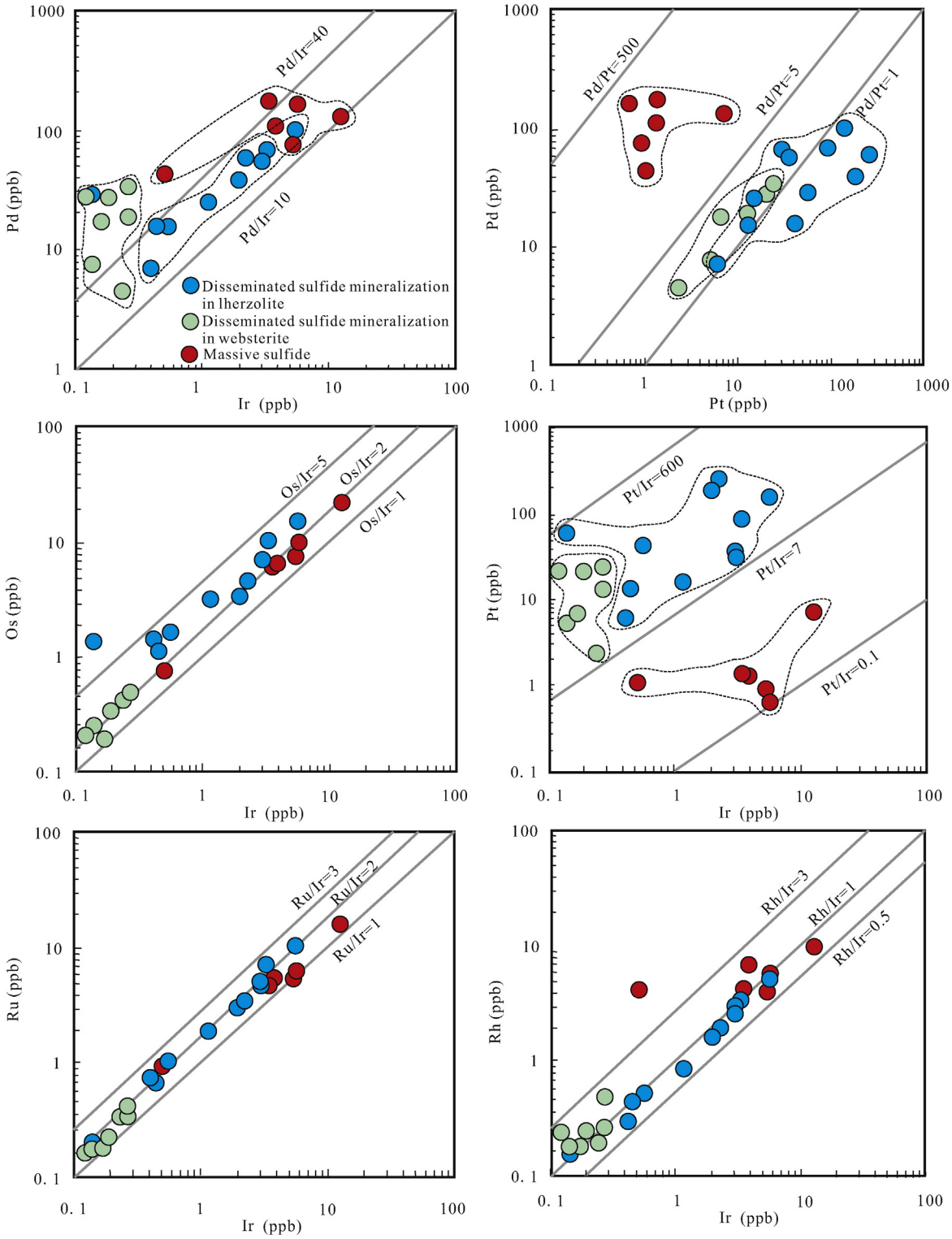


**Fig. 7.** Plots of Pt vs. Pd, and Ir vs. Pd, Os, Ru and Rh for sulfide mineralization from the Huangshannan Intrusion. Data for the lherzolite-hosted sulfide mineralization are from Zhao et al. (2015).

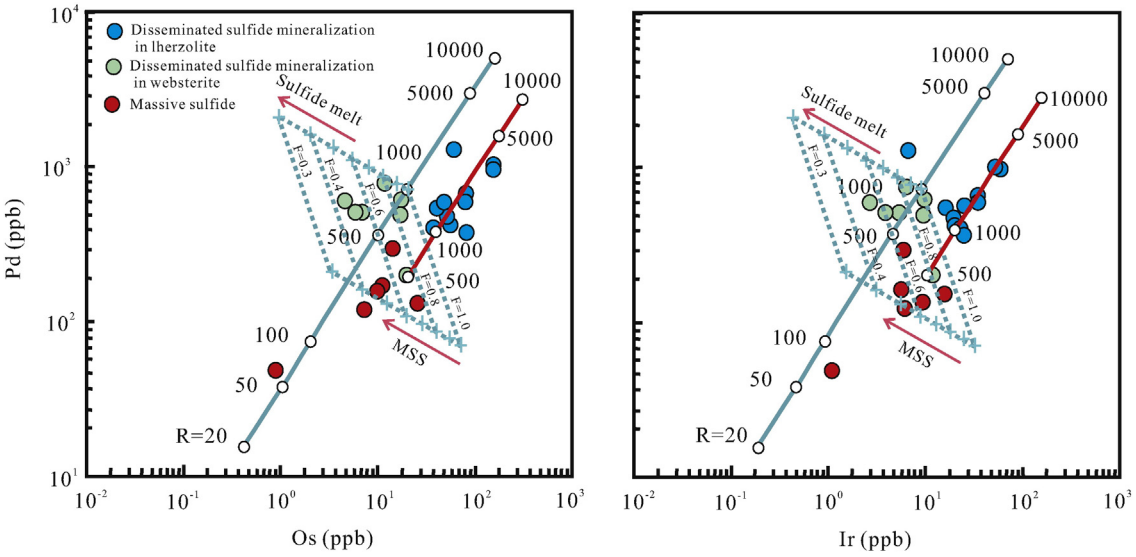


**Fig. 8.** Plots of Pd vs. Ir and Os tenors for sulfide mineralization from the Huangshannan Intrusion. F = the fraction of remaining sulfide liquid during fractional crystallization of monosulfide solid solution (MSS) from sulfide liquid.

formed the websterite (Fig. 8). On the other hand, the sulfide mineralization in the lherzolite and websterite shows a negative correlation between the Ni/Cu and Cu/Pd ratios, indicating different parental magma types rather than evolution from a common parental magma (Zhao et al., 2015). In summary, the Huangshannan Intrusion was formed by multiple magma pulses and magmas for lherzolite and websterite were derived from different sources or have different contributions of mantle versus crustal material.

### 7.2. Sources of the anomalously Ni-rich parental magmas

Compared to many important magmatic Ni–Cu deposits, olivine grains from the lherzolite from the Huangshannan intrusion have significantly higher Ni but similar Fo contents (Fig. 9a). The Ni–Fe exchange between olivine and sulfide liquid may contribute to the anomalously high Ni contents in the olivine. However, the olivine grains in sulfide show similar or lower Ni contents than the poikilitic olivine crystals and olivine inclusions in either the mineralized or the unmineralized samples (Fig. 9b). Another possibility is that the Ni–Fe exchange may have occurred in the sulfide-saturated magma and then sulfide melts settled out of the magma column. Thus, the poikilitic olivine grains and olivine inclusions may have experienced Ni–Fe exchange and, therefore, the Ni content of the olivine is increased markedly. However, sulfides may segregate from the parental magma in different stages and the amount of sulfide formed and possibly removed is small when compared to the amount of olivine crystallization. Thus, Ni–Fe exchange between olivine and sulfide would generate Ni-rich zonation of the olivine crystals; this is inconsistent with the anomalously high Ni contents in whole olivine grains in the Huangshannan Intrusion. The small sulfide content of the magma is not likely to explain the elevated Ni content of the olivine grains in either the mineralized or the unmineralized samples. In summary, the Ni–Fe exchange between olivine and sulfide liquid cannot explain the anomalously high Ni contents in the olivine grains from the Huangshannan Intrusion.

Assuming a partition coefficient for Ni between olivine and magma to be 7 (Naldrett, 2004) and associating it with the Ni content of olivine in the lherzolite (1540–4023 ppm), it is possible to estimate the Ni content of the parental magmas. Our data yield estimates of 220–575 ppm

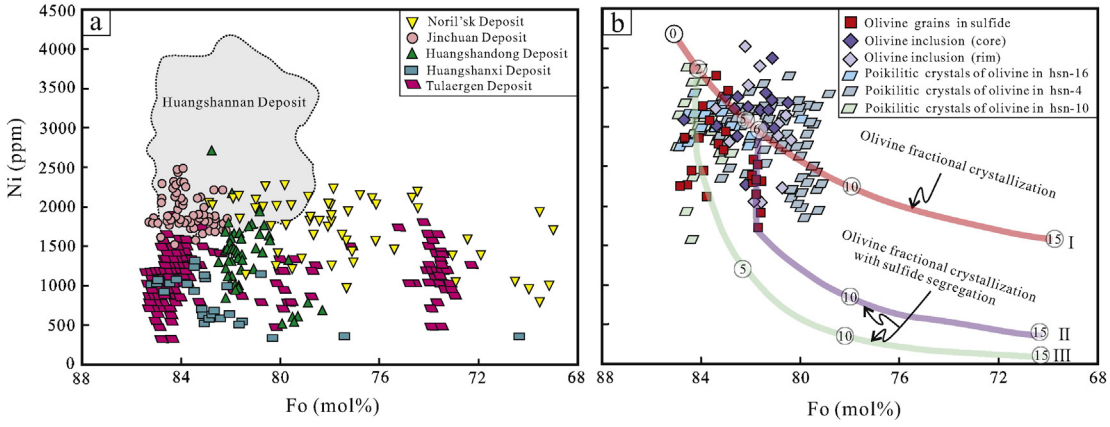


**Fig. 9.** (a) Composition of olivine in the Huangshannan Intrusion, compared to olivines from a range of mineralized intrusions elsewhere. Sources of data: Noril'sk: Li et al. (2003); Jinchuan: Li et al. (2004); Huangshanxi: Zhang et al. (2011); Huangshandong: Deng et al. (2012); and Tulaergen: Sun (2009). (b). Ni and Fo contents of olivine in lherzolite from the Huangshannan Intrusion, and models of fractional crystallization. We assume that the parental magma contains 9.1 wt.% FeO, 8.7 wt.% MgO and 600 ppm Ni. Olivine fractional crystallization is simulated assuming olivine-magma $D_{Ni(olivine/magma)} = 7$ (Naldrett, 2004) and $(FeO/MgO)_{olivine}/(FeO/MgO)_{magma} = 0.3$ (Roeder and Emslie, 1970). The sulfide/magma partition coefficient of Ni ($D_{Ni(sulfide/magma)}$) is 500 (Barnes and Maier, 1999). Circles with numbers, like 0.2, represent the degree of fractional crystallization of olivine. I is the curve of olivine fractional crystallization; II is the curve of modeling 2% olivine crystallization from the parental magma, and then olivine and sulfide simultaneously separated (olivine/sulfide = 25/1); III is the curve of modeling 6% olivine crystallization from the parental magma, and then olivine and sulfide simultaneously separated (olivine/sulfide = 50/1).

Ni with a mean of 415 ppm Ni for the parental magma from which the olivine crystallized. The parental magma of the Huangshannan Intrusion is believed to have had a high Mg basaltic composition (see details in Section 7.3). However, the calculated Ni content of this parental magma is much higher than those of many high Mg basaltic parental magmas that crystallized olivine with similar Fo contents compared to the Huangshannan Intrusion (Fig. 9a), such as the Noril'sk (300 ppm, Li et al., 2003), Huangshandong (260 ppm, Deng et al., 2012; 250 ppm, Gao et al., 2013) and Jinchuan Intrusions (330 ppm, Li et al., 2004). Therefore, the Huangshannan Intrusion is inferred to have been sourced from Ni-rich parental magmas.

Two possible mechanisms may account for the Ni enrichment of the parental magma, viz.: 1. Generation of the magma from a "pyroxenitic" mantle source (Sobolev et al., 2007). 2. Upgrading of the Ni content of the parental magma by a process of upgrading and scavenging of metals from previously formed sulfide melts (Kerr and Leitch, 2005). Magmas derived from a "pyroxenitic" mantle source are predicted to have higher Ni concentrations (by a factor of 1.5 to 2) than normal tholeiites for a typical mantle range of Fo contents (89–91 mol.%; Sobolev et al., 2007). This mechanism has been used to explain the high Ni contents of the olivines and parental magmas for the Gudchikhinskaya Formation in the Noril'sk Region (Sobolev et al., 2007) and for the Santa Rita sulfide zone within the Fazenda Mirabela Intrusion (Barnes et al., 2013). The highest Fo content (84.92 mol.%) of olivine from the Huangshannan Intrusion is much lower than the Fo contents of olivines in equilibrium with primitive mantle-derived magmas. The Kevitsa Intrusion in the Central Lapland greenstone belt of Northern Finland shows extremely high Ni contents in olivines, which is considered to originate from a Ni-rich basaltic magma by assimilation of a pre-existing Ni–Cu sulfide deposit (Yang et al., 2013). However, this mechanism may not be applicable for the Huangshannan Deposit due to the lack of any known pre-existing Ni–Cu sulfide deposits in the Huangshannan Intrusion. As discussed above, the symmetric and reproducible variations of both Fo and Ni contents of olivine grains from core to margin indicate that the lherzolite has been formed by different magma pulses. The sulfide melts formed from any previous injections of magma may be assimilated by new magma pulses, thus producing new parental magmas enriched in Ni (Kerr and Leitch, 2005). This mechanism should also cause an upgrading in PGE tenors, consistent with the high PGE tenors in the Huangshannan Deposit (e.g., Zhao et al., 2015). Thus, the anomalously Ni-rich composition of the parental magmas of the Huangshannan Intrusion is created from moderately Ni-rich primary magmas by a process of upgrading and scavenging of metals from previously formed sulfide melts.

### 7.3. The formation of sulfide mineralization in the lherzolite

The compositions of olivine from a range of mineralized intrusions are compared in Fig. 9a. The olivine grains in lherzolite from the Huangshannan Intrusion have significantly higher Ni and moderately high Fo contents (Fig. 9a). The method of Chai and Naldrett (1992b) was used to calculate the parental magma composition for these olivines. Using the composition of olivine with the highest Fo content (84.92 mol.%), olivine-magma Fe–Mg exchange coefficient or $(FeO/MgO)_{olivine}/(FeO/MgO)_{magma} = 0.3$ (Roeder and Emslie, 1970), and the LOI- and sulfide-free whole-rock compositions of lherzolite samples (Zhao et al., 2015), the parental magma is estimated to contain 9.1 wt.% FeO and 8.7 wt.% MgO. The MgO content of the parental magma estimated by the method of Chai and Naldrett (1992b) has a positive correlation with the highest Fo content used for calculation. Thus, the MgO content calculated in this method may be lower than the true MgO content of the parental magma for two reasons, viz.: 1. The highest Fo content measured in this study may not be typical of the highest Fo content in the Huangshannan Intrusion. 2. The Fo content may decrease because of a re-equilibration between the olivine and interstitial silicate magma. In summary, the Huangshannan Intrusion was likely derived from a high Mg basaltic parental magma (MgO > 9 wt.%).

Based on the modeling using the composition of the most Fo-rich olivine, we propose that the parental magma for the Huangshannan Intrusion contains 9.1 wt.% FeO, 8.7 wt.% MgO and 600 ppm Ni. These FeO and MgO contents are lower than the parental magma compositions of the Huangshandong (13.5 wt.% FeO, 11.2 wt.% MgO, Deng et al., 2012), Tulaergen (12 wt.% FeO, 12.5 wt.% MgO, Sun, 2009) and Jinchuan Deposits (11.2 wt.% FeO, 11.5 wt.% MgO, Chai and Naldrett, 1992a; Li et al., 2004; 12.42 wt.% FeO, 12.33 wt.% MgO, Li and Ripley, 2011). The Ni content of the parental magma of the Huangshannan Intrusion is consistent with the modeling of the Zhao et al. (2015), but it is much higher than those of the Noril'sk (300 ppm, Li et al., 2003), Huangshandong (260 ppm, Deng et al., 2012; 250 ppm, Gao et al., 2013) and Jinchuan Intrusions (330 ppm, Li et al., 2004).

Rayleigh fractionation equation has been used to describe models for the evolution of the parental magma that formed the lherzolite. Fig. 9b shows that the parental magma may have undergone 2% olivine crystallization and then the evolved magma became sulfide-saturated (Curve II, Fig. 9b). The separated olivine (olivine grains in sulfide) and segregated sulfides are calculated in a ratio of olivine/sulfide = 25/1. Subsequently, the parental magma became sulfide-saturated again after 6% crystallization of olivine (Curve III, Fig. 9b). The crystallized olivine grains (olivine grains in sulfide) and segregated sulfide melts are in a ratio of olivine/sulfide = 50/1. Most of the poikilitic olivine crystals and olivine inclusions from the lherzolite plot close to the model line of olivine crystallization (Curve I, Fig. 9b).

### 7.4. Genetic model of the Huangshannan Deposit

The Huangshannan Intrusion was formed in different magma pulses (Zhao et al., 2015). The anomalously Ni-rich composition of the parental magma of the lherzolite is created from a moderately Ni-rich primary magma by a process of upgrading and scavenging of metals from previously formed sulfide melts. The parental magma that formed the lherzolite has experienced previous sulfide segregation and olivine crystallization.

A second magma pulse ascended into the magma chamber and formed the websterite. Massive sulfides can be attributed to MSS-sulfide liquid fractionation from this second magma pulse. The third magma pulse was emplaced in both the western and eastern parts of the Huangshannan Intrusion and formed the mafic unit which contains no significant mineralization.

## 8. Conclusions

(1) The anomalously Ni-rich composition of the parental magmas of the Huangshannan Intrusion is created from moderately Ni-rich primary magmas by a process of upgrading and scavenging of metals from previously formed sulfide melts.
(2) The parental magma that formed the lherzolite has experienced previous sulfide segregation and olivine crystallization.

## Conflict of interest

We declare that we do not have any commercial or associative interest that represents a conflict of interest in connection with the work submitted.

## Acknowledgments

We thank Jiaquan Yang of the Hami Great Wall Industry Co., Ltd. for his assistance in the field work. The authors extend their profound gratitude to He Rong for his assistance in electron microprobe analysis at

the Chinese Academy of Geological Sciences. We especially thank Yu-Feng Deng of the Hefei University of Technology for his enthusiastic help in the modeling of olivine crystallization. An earlier draft of this paper was improved by the thoughtful comments and suggestions from David Symons, Guoxiang Chi and Jianfeng Gao. Constructive reviews by an anonymous reviewer and the Associate Editor Peter C. Lightfoot are greatly appreciated. This study was financially supported by the National Natural Science Foundation of China (U1303292), the National Science and Technology Support Program of China (No. 2011BAB06B02), the Fundamental Research Funds for the Central Universities (No. 53200859399) and the China Geological Survey (No. 121211220926 and 12120113089400).

## References

Asif, M., Parry, S.J., 1991. Study of the digestion of chromite during nickel sulphide fire assay for the platinum group elements and gold. Analyst 116, 1071–1073.
Barnes, S.J., 1986. The effect of trapped liquid crystallization on cumulus mineral compositions in layered intrusions. Contrib. Mineral. Petrol. 93, 524–531.
Barnes, S.J., Lightfoot, P.C., 2005. Formation of magmatic nickel sulfide ore deposits and processes affecting their copper and platinum group element contents. Econ. Geol. 100th Anniversary Volume, 179–213.
Barnes, S.J., Maier, W.D., 1999. The fractionation of Ni, Cu and the noble metals in silicate and sulfide liquids. Geol. Assoc. Can. Short Course Notes 13, 69–106.
Barnes, S.J., Godel, B., Gürer, D., Brenan, J.M., Robertson, J., Paterson, D., 2013. Sulfide-olivine Fe-Ni exchange and the origin of anomalously Ni rich magmatic sulfides. Econ. Geol. 108, 1971–1982.
Campbell, I.H., Naldrett, A.J., 1979. The influence of silicate: sulfide ratios on the geochemistry of magmatic sulfides. Econ. Geol. 74, 1503–1506.
Chai, G., Naldrett, A.J., 1992a. Characteristics of Ni–Cu-PGE mineralization and genesis of the Jinchuan deposit, Northwest China. Econ. Geol. 47, 1475–1495.
Chai, G., Naldrett, A.J., 1992b. The Jinchuan ultramafic intrusion: cumulate of a high-Mg basaltic magma. J. Petrol. 33, 277–303.
Chen, L.M., Song, X.Y., Danyushevsky, L.V., Xiao, J.F., Li, S.B., Guan, J.X., 2009. Correlation between Ni and MgO contents of olivine in segment of the Jinchuan intrusion, NW China, and its geological implication. Acta Petrol. Sin. 25, 3369–3378 (in Chinese with English abstract).
Chen, L.M., Song, X.Y., Reid, R.K., Tian, Y.L., Wang, Y.S., Deng, Y.F., Xiao, J.F., 2013. Segregation and fractionation of magmatic Ni–Cu-PGE sulfides in the Western Jinchuan Intrusion, Northwestern China: insights from platinum group element geochemistry. Econ. Geol. 108, 1793–1811.
Corfu, F., Lightfoot, P.C., 1996. U–Pb geochronology of the sublayer environment, Sudbury igneous complex, Ontario. Econ. Geol. 91, 1263–1269.
Deng, Y.F., Song, X.Y., Zhou, T.F., Yuan, F., Chen, L.M., Zheng, W.Q., 2012. Correlations between Fo number and Ni content of olivine of the Huangshandong Intrusion, eastern Tianshan, Xinjiang, and the genetic significances. Acta Petrol. Sin. 28, 2224–2234 (in Chinese with English abstract).
Gao, J.F., Zhou, M.F., Lightfoot, P.C., Wang, C.Y., Qi, L., Sun, M., 2013. Sulfide saturation and magma emplacement in the formation of the Permian Huangshandong Ni–Cu sulfide deposit, Xinjiang, NW China. Econ. Geol. 108, 1833–1848.
Guan, J.X., Song, X.Y., Danyushevsky, L.V., Chen, L.M., Nie, X.Y., 2010. Genetic significances of olivine from magmatic sulfide ore-bearing intrusionsin central zone of Emeishan Large Igneous Province. Earth Sci. J. China Univ. Geosci. 35, 224–234 (in Chinese with English abstract).
Jahn, B.M., Windley, B., Natal'in, B., Dobretsov, N., 2004. Phanerozoic continental growth in Central Asia. J. Asian Earth Sci. 23, 599–603.
Kerr, A., Leitch, A.M., 2005. Self-destructive sulfide segregation systems and the formation of high-grade magmatic ore deposits. Econ. Geol. 100, 311–332.
Li, C., Ripley, E.M., 2011. The Jinchuan Ni–Cu-(PGE) deposit: tectonic setting, magma evolution, ore genesis, and exploration implications. Soc. Econ. Geol. Spec. Publ. 17, 164–180.
Li, C., Naldrett, A.J., Ripley, E.M., 2007. Controls on the Fo and Ni contents of olivine in sulfide-bearing mafic-ultramafic intrusions: principles, models and examples from Voisey's Bay. Earth Sci. Front. 14, 177–185.
Li, C., Ripley, E.M., Naldrett, A.J., 2003. Compositional variations of olivine and sulfur isotopes in the Norilsk and Talnakh intrusions, Siberia: implications for ore forming processes in dynamic magma conduits. Econ. Geol. 98, 69–86.
Li, C., Xu, Z.H., de Waal, S.A., Ripley, E.M., Maier, W.D., 2004. Compositional variations of olivine from the Jinchuan Ni–Cu sulfide deposit, Western China: implications for ore genesis. Mineral. Deposita 39, 159–172.
Lightfoot, P.C., Evans-Lamswood, D., 2015. Structural controls on the primary distribution of mafic-ultramafic intrusions containing Ni–Cu-Co-(PGE) sulfide mineralization in the roots of large igneous provinces. Ore Geol. Rev. 64, 354–386.
Lightfoot, P.C., Keays, R.R., Doherty, W., 2001. Chemical evolution and origin of Ni sulfide mineralization in the Sudbury Igneous Complex, Ontario, Canada. Econ. Geol. 96, 1855–1876.
Lightfoot, P.C., Keays, R.R., Morrison, G.G., Bite, A., Farrell, K.P., 1997. Geochemical relationships in the Sudbury Igneous Complex; origin of the main mass and offset dikes. Econ. Geol. 92, 289–307.
Likhachev, A.P., 1994. Ore-bearing intrusions of the Noril'sk region. Ont. Geol. Surv. Spec. Publ. 5, 185–202.
Mao, Y.J., Qin, K.Z., Li, C., Tang, D.M., 2014. A modified genetic model for the Huangshandong magmatic sulfide deposit in the Central Asian Orogenic Belt, Xinjiang, Western China. Mineral. Deposita 50, 65–82.
McDonough, W.F., Sun, S.S., 1995. The composition of the earth. Chem. Geol. 120, 223–253.
Naldrett, A.J., 1998. World-class Ni–Cu-PGE deposits: key factors in their genesis. Mineral. Deposita 34, 227–240.
Naldrett, A.J., 2004. Magmatic sulfide deposits: geology, geochemistry and exploration. Springer-Verlag, Berlin Heidelberg, pp. 1–727.
Naldrett, A.J., Duke, J.M., Lightfoot, P.C., Thompson, J.F.H., 1984. Quantitative modelling of the segregation of magmatic sulphides: an exploration guide. CIM Bull. 77, 46–56.
Roeder, P.L., Emslie, R.F., 1970. Olivine–liquid equilibrium. Contrib. Mineral. Petrol. 71, 257–269.
Sengör, A.M.C., Natal'in, B.A., Burtman, V.S., 1993. Evolution of the altaid tectonic collage and Paleozoic crustal growth in Eurasia. Nature 364, 299–307.
Sobolev, A.V., Hoffman, A., Kuzmin, D., Yaxley, G., Arndt, N., Chung, S.-L., Danyushevsky, L., Elliott, T., Frey, F., Garcia, M., Gurenko, A., Kamenetsky, V., Kerr, A., Krivolutskaya, N., Matvienkov, V., Nikogosian, I., Rocholl, A., Sigurdson, I., Sushchevskaya, N., Teklay, M., 2007. The amount of recycled crust in sources of mantle-derived melts. Science 316, 412–417.
Su, B.X., Qin, K.Z., Sun, H., Tang, D.M., Xiao, Q.H., Cao, M.J., 2009. Petrological and mineralogical characteristics of Hongshishan mafic-ultramafic complex in Beishan area, Xinjiang: implications for assimilation and fractional crystallization. Acta Petrol. Sin. 25, 873–887 (in Chinese with English abstract).
Su, B.X., Qin, K.Z., Sun, H., Tang, D.M., Xiao, Q.H., Liu, P.P., 2012. Olivine compositional mapping of mafic-ultramafic complexes in Eastern Xinjiang (NW China): implications for Cu–Ni mineralization and tectonic dynamics. J. Earth Sci. 23, 41–53.
Su, B.X., Qin, K.Z., Sun, H., Wang, H., 2010. Geochronological, petrological, mineralogical and geochemical studies of the Xuanwoling mafic-ultramafic intrusion in the Beishan area, Xinjiang. Acta Petrol. Sin. 26, 3283–3294 (in Chinese with English abstract).
Su, B.X., Qin, K.Z., Tang, D.M., Deng, G., Xiao, Q.H., Sun, H., Lu, H.F., Dai, Y.C., 2011. Petrological features and implications for mineralization of the Poshi mafic-ultramafic intrusion in Beishan area, Xinjiang. Acta Petrol. Sin. 27, 3627–3639 (in Chinese with English abstract).
Sun, H., 2009. Ore-Forming Mechanism in Conduit System and Ore-Bearing Property Evaluation for Mafic–Ultramafic Complex in Eastern Tianshan, Xinjiang. Institute of Geology and Geophysics, Chinese Academy of Sciences (Ph. D thesis in Chinese with English abstract).
Sun, T., Qian, Z.Z., Deng, Y.F., Li, C.S., Song, X.Y., Tang, Q.Y., 2013. PGE and isotope (Hf-Sr-Nd-Pb) constraints on the origin of the Huangshandong magmatic Ni–Cu sulfide deposit in the Central Asian Orogenic Belt, Northwestern China. Econ. Geol. 108, 1849–1864.
Wang, R.M., Liu, D.Q., Yin, D.T., 1987. The conditions of controlling metallogeny of Cu, Ni sulphide ore deposits and the orientation of finding ore of Hami, Xinjiang, China. Miner. Rock 1, 115–121 (in Chinese).
Wang, Y.W., Wang, J.B., Wang, L.J., 2006. Comparison of host rocks between two vanadic titianomagnetite deposit types from the eastern Tian-shan mountains. Acta Petrol. Sin. 22, 1425–1436 (in Chinese with English abstract).
Xia, M.Z., Jiang, C.Yi., Li, C.S., Xia, Z.D., 2013. Characteristics of a newly discovered Ni–Cu sulfide deposit hosted in the poyi ultramafic intrusion, Tarim Craton, NW China. Econ. Geol. 108, 1865–1878.
Xiao, W.J., Windley, B.F., Yuan, C., Sun, M., Han, C.M., Lin, S.F., Chen, H.L., Yan, Q.R., Liu, D.Y., Qin, K.Z., Li, J.L., Sun, S., 2009. Paleozoic multiple subduction–accretion processes of the southern Altaids. Am. J. Sci. 309, 221–270.
Xie, W., Song, X.Y., Deng, Y.F., Chen, L.M., Zhang, X.Q., Zheng, W.Q., Wei, X., 2013. Geology and olivine geochemistry of the Heishan Ni–Cu-(PGE) sulfide deposit, Gansu, NW China. Acta Petrol. Sin. 29, 3487–3502.
Yang, S.H., Maier, W.D., Hanski, E.J., Lappalainen, M., Santaguida, F., Määttä, S., 2013. Origin of ultra-nickeliferous olivine in the Kevitsa Ni–Cu-PGE-mineralized intrusion, northern Finland. Mineral. Deposita 166, 81–95.
Zhang, M.J., Li, C.S., Fu, P.A.E., Hu, P.Q., Ripley, E.M., 2011. The Permian Huangshanxi Cu–Ni deposit in Western China: intrusive-extrusive association, ore genesis, and exploration implications. Mineral. Deposita 46, 153–170.
Zhao, Y., Xue, C.J., Zhao, X.B., Yang, Y.Q., Ke, J.J., 2015. Magmatic Cu–Ni sulfide mineralization of the Huangshannan mafic-ultramafic intrusion, Eastern Tianshan, China. J. Asian Earth Sci. 105, 155–172.